Quantifying the role of shade on microclimate conditions and water use efficiency of a subalpine wetland in the Canadian Rocky Mountains, Kananaskis, Alberta

by

Dylan Matthew Hrach

A thesis

presented to the University of Waterloo

in fulfillment of the

thesis requirement for the degree of

Master of Science

in

Geography (Water)

Waterloo, Ontario, Canada, 2019

Author's Declaration

I hereby declare that I am the sole author of this thesis. This is a true copy of the thesis, including any required final revisions as accepted by my examiners.

I understand that my thesis may be made electronically available to the public.

Abstract

Alpine regions contribute 60 % of annual surface runoff, playing an important role in regulating the global water balance. Many of the world's major river networks originate from alpine headwater basins, popularizing mountains as the "Water Towers of the World". The Rocky Mountains represent Western Canada's "Water Tower" since they store and distribute water resources to over 13 million people across Western Canada and the Pacific Northwest USA. At the headwater, topography causes land surfaces to cycle in and out of shadows, creating distinct microclimates that strongly influence evapotranspiration (ET) and carbon fluxes. Yet, relatively few studies have observed the relationship between the energy, water, and carbon fluxes of mountain catchments; and have rather focused on periods of snow and ice cover. Therefore, understanding the contribution of subalpine wetlands to the water budget remains a leading hydrological need in mountain areas worldwide.

This thesis attempts to address these knowledge gaps by investigating the influence of complex terrain on the spatial and temporal variability of shade across a subalpine wetland (2,083 m a.s.l.) in the Canadian Rocky Mountains and the effect of shade on seasonal flux dynamics. Meteorological and eddy covariance equipment was installed from June 7th to September 10th to establish baseline environment conditions and to monitor the turbulent and radiative fluxes over the 2018 snow free period. Hill shade and solar radiation models for clear-sky days were compared to field observations to understand how shade impacted the energy, water, and carbon fluxes. Water Use Efficiency (WUE) was used as a metric to understand the relationship between water and carbon cycling.

Overall, shade shortened the growing season and prolonged snowmelt. Shade was greatest near the headwall and reduced cumulative solar radiation by 86.4 MJ over the study period. When shade was low and constant during the period of *Stable Shade* (June 7th – July 30th), it had a non-significant relationship with incoming solar radiation (K↓) and net radiation (Q*); however, when shade rapidly increased during the period of *Dynamic Shade* (July 31st – September 10th) it strongly influenced K↓ and Q*. On average, during *Dynamic Shade*, each hourly increase of shade per day, reduced K↓ and Q* by 32 W/m^2 and 28 W/m^2, equivalent to 13 % and 16 %, respectively. Water and carbon fluxes had a similar response to shade as the energy fluxes. Each hourly increase of shade reduced ET and Gross Primary Production (GPP) by similar margins: 17 % and 15 %,

respectively. Therefore, WUE remained relatively unaffected by horizon shade, because shade equally reduced ET and GPP. These findings indicate that under uncertain future climate scenarios (i.e. increased risk of flood, drought, and forest fires), shade may be an important mechanism for moisture conservation in a variety of subalpine ecosystems that are at risk of late season water stress.

Acknowledgements

In the spirit of reconciliation, I acknowledge that this research was conducted on the traditional territories of the Blackfoot Confederacy (Siksika, Kainai, Piikani), the Tsuut'ina, the Îyâxe Nakoda Nations, the Métis Nation (Region 3), and all people who make their homes in the Treaty 7 region of Southern Alberta (Calgary Foundation, 2019).

There are many individuals, groups, and organisations who helped contribute to this thesis and my personal/professional development over the last several years. First and foremost, I would like to thank my supervisor Dr. Rich Petrone. In 2015 you gave me the opportunity to work at a remote field site as an undergraduate student. URSA taught me a lot about myself and what I was capable of under harsh living (and working) conditions. When the opportunity presented itself to pursue graduate studies in the mountains, it was too good to pass up. I am forever grateful that you took a chance on this undergrad in 2015 and for your continued belief, endless support, and perfectly placed one liners.

Thank you to those who worked tirelessly in data collection and compilation. Thank you, Jessica Williamson, Lindsey Langs, and Sheryl Chau, for the hard labour and optimistic spirits you brought every day to help complete such an intensive field project. Thank you to Brandon Van Huizen for your support in completing the hill shade model and for allowing me to be your "trial dummy". Thanks to Dr. Myroslava Khomik and Adam Green for your endless advice and expertise in processing and troubleshooting eddy covariance data. Thank you to all other members of the Hydrometeorology Research Group for your valuable input during our weekly lab meetings. Finally, shout out to Tyler Prentice and Jessica Williamson for our long days in the dungeon battling R together, we made quite the team.

Thank you to the shareholders of Fortress Mountain Resort and their management team for site access, logistical support, and wildlife awareness. Special thanks to Mel Folden for your welcoming smile and positive energy. The conversations and laughs we shared will never be forgotten, n'or will the seemingly endless garlic shrimp after those long days in the field.

To friends and colleagues that I met along the way in CREATE for Water Security, the Water Institute, and GWF-YP, this is just the beginning. I look forward to the exciting careers we share together. I would like to send a special shout out to Kan Fam 2018 and my team members on Trippin' Balls for making this such a rewarding experience.

To my family, thank you mom and dad for your continued support in pursuit of my passion. Thank you to my sister Alex for keeping me mentally fresh by reviewing her papers that had nothing to do with alpine hydrology. Finally, thank you Kendra for everything you've done over the last two and a half years, your love, support, and encouragement was unwavering.

Table of Contents

List of Figures

List of Tables

Chapter 1: General Introduction

1.0 Review of Key Literature

1.1 Alpine Hydrology: Global and Local Contexts

Alpine regions play an important role in regulating the global water balance. Despite only covering approximately 20 % of the Earth's terrestrial surface (Ives & Messerli, 1999), they contribute 40 to 60 % of annual surface runoff (Grusson et al. 2015). Therefore, many of the world's major river networks originate from alpine sourced headwater basins, where downstream runoff from snowmelt may entirely comprise regional stream flow (Viviroli et al. 2011). Approximately 40 % of the global population lives in watersheds sourced from alpine headwater rivers which is the primary drinking water supply for over 16 % of those residents (Meybeck et al. 2001; Barnett et al. 2005). In the Western United States and Canada alone, over 60 million people rely on spring snowmelt from mountains as their primary water source for irrigation and municipal water supplies (Bales et al. 2006). Mountains also provide a disproportionate amount of runoff compared to low lying valley regions and offer many ecosystem services at a range of spatial scales (European Environment Agency, 2010). In areas that receive minimal precipitation during the summer months (i.e. the semi-arid Western USA and Canada), seasonal snow packs provide a natural and continuous water source for downstream users during dry summer and fall seasons (Barnett et al. 2005). Thus, many have popularized mountain regions as the "Water Towers of the World", vocabulary often used in literature to describe the Swiss Alps and the Himalayan Mountains (European Environment Agency, 2009; Immerzeel, 2008).

The Rocky Mountains are Western Canada's Water Tower, since they store and distribute large quantities of water resources across the prairie provinces. The Canadian Rockies are the primary water source for over 13 million people who reside in the provinces of British Columbia, Alberta, Saskatchewan, and Manitoba in addition to the states of Washington and Oregon (Fang et al. 2013). Runoff from the Rockies supplies the Athabasca, Saskatchewan, Columbia, and Fraser Rivers, all important headwater resources for agriculture, the generation of hydroelectricity, municipal water sources, and industry operations downstream (Fang et al. 2013). The South Saskatchewan River Watershed is an example of a basin where municipal water supply and downstream industry are heavily reliant on the Rocky Mountains (Figure 1-1).
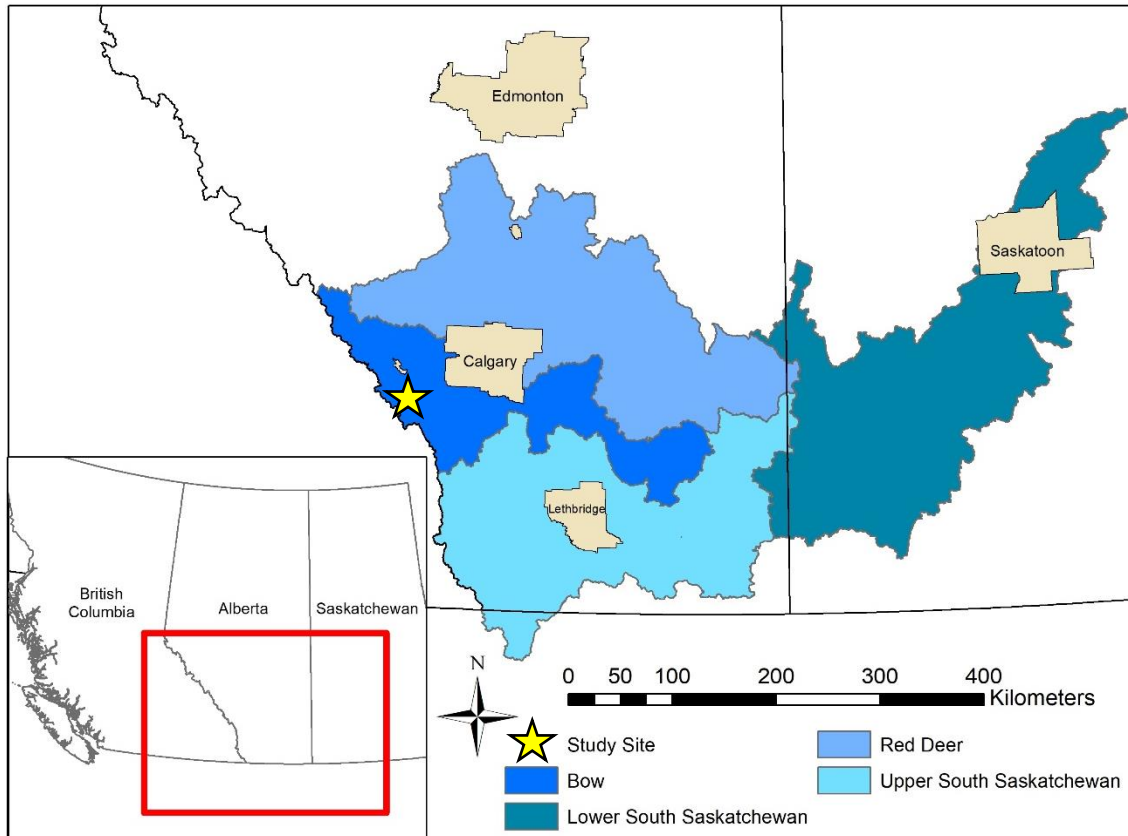
Figure 1-1: South Saskatchewan River Basin drainage area. Major sub-watersheds are shown (Bow, Red Deer, Lower and Upper South Saskatchewan) and major cities (Data sources: Municipal boundaries, Statistics Canada (2016); Watershed boundaries, Government of Alberta (2018)).

1.2 Alpine Climate: Global and Local Contexts

Alpine climates differ from that of lowlands due to their geographic and environmental setting. There are four geographic features that strongly influence mountain climates, defined in Barry (1981) as: (i) latitude; (ii) continentality; (iii) altitude; and (iv) topography.

Latitude influences the annual and seasonal cycles of temperature and precipitation that mountain areas receive (Beniston, 2006). Increased latitude decreases the net radiation and temperature, which decreases the tree- and snow-line elevations (Barry, 1981). Latitude plays a strong role in regulating temperature because mid- to high latitudes have a greater fluctuation in seasonal and diurnal climate (Barry, 1981). For example, Niwot Ridge, Colorado experiences a seasonal temperature range of 21 °C and a diurnal temperature gradient of 6 to 8 °C depending on time of year (Barry, 1973). Latitude also influences the type and amount of precipitation; in middle

2

to upper latitudes there is a well-defined winter season with prolonged periods of freezing temperatures and snow cover, resulting in over 80 % of their annual precipitation falling as snow (Geiger, 1965).

Continentality is the proximity of a region to the ocean, and the influence of maritime climate on the landscape. Therefore, mountains located inland (continental) have vastly different climates than those along the coast (maritime). Continental mountains receive more sunshine (increased available radiative energy), less precipitation, and have a greater seasonal and diurnal temperature range (Beniston, 2006). The treeline in continental mountains is often at higher elevations, influencing plant biodiversity in these regions (Beniston, 2006).

Altitude is another important characteristic influencing mountain climate because atmospheric density, pressure and temperature each follow a decreasing trend with increasing height into the troposphere (Beniston, 2006). Altitude also strongly influences radiation, wind, and precipitation (Barry, 1973). Diurnal and seasonal air temperature ranges decrease with altitude because the atmosphere has a lower heat capacity at increased elevations (Beniston, 2006). Studies in the Rocky Mountains have found that increases in elevation have often resulted in decreases in temperature but increases in precipitation (Millar et al. 2017). Therefore, the distribution of ecosystems in mountain regions have a strong relationship with altitude (Beniston, 2006). In fact, the relationship is so strong that mountain climate zones have been defined by the transition of vegetation within elevation bands (Beniston, 2006).

The final geographic feature outlined by Barry (1981) is topography, which is an important control on local mountain climates because slope, aspect, and land surface exposure redistribute solar energy and influence how (and when) it reaches the surface (Beniston, 2006). Aspect determines whether a surface will receive any incident radiation; while the surrounding topography may act as a barrier to block radiation from reaching the surface (Beniston, 2006). Depending on the sun's azimuth within the sky, the topographic barrier may shade different areas at different times of the year. Topography may also influence the amount and type of precipitation over mountain regions. Mountains behave like a barrier that forces moist air upward until it reaches the condensation level and creates mist, fog, clouds, and precipitation (Beniston, 2006). Therefore, precipitation often occurs on the windward side of the mountain due to complexities associated with uplift (Beniston, 2006).

1.3 Alpine Climate: Climate Change

Climate change is an evolving threat to extreme ecosystems where vegetation exists at the extent of its environmental tolerance limits (Bavay et al. 2015). Alpine environments are examples of extreme ecosystems because complex terrain restricts light, temperature, and/or moisture available to the surface (Barros et al. 2017). Confirmed by the Fourth Assessment Report published by the Intergovernmental Panel on Climate Change (IPCC 4AR), research has found that warming in extreme environments will be greatest in northern latitudes and upper alpine basins. The report found that the global average air temperature increased by an average of 0.6 °C over the 20th century (IPCC, 2001), and that temperatures in the alpine zone rose over 1.2 °C during the same period (Böhm et al. 2001).

Recent studies have found that temperatures in Canada have been warming at double the global rate, with even greater rates in upper altitudes and latitudes (Bush & Lemmen, 2019). Increased temperatures in mountain landscapes, associated with climate change, have already led to earlier spring snowmelt and runoff, a decreased snowpack, and an increase in winter rain on snow events (Regonda et al. 2004; Christensen & Lettenmaier, 2007; Ashfaq et al. 2013). Due to increasingly harsh climates, shorter growing seasons, and the shift in key hydrological events, it will become increasingly difficult for current alpine ecosystems to adapt to new climate extremes and pressing ecological disturbances (Baron et al. 2009). Many regions within the North American Rocky Mountains have begun to experience climate change, including increased drought, fire, and insect outbreak like the mountain pine beetle (Desai et al. 2011; Rood et al. 2008). Because mountains are highly susceptible to negative impacts associated with climate change, further research is required on understanding their ecohydrological characteristics (Beniston, 2003).

1.4 Alpine Wetlands and Vegetation

An accurate estimate of the global extent of alpine wetlands does not yet exist; however, environmental conditions within mountain terrain promote the establishment of wetlands in alpine stretches, such as intermountain basins and high mountain valleys (Windell et al. 1986). Alpine wetlands play a significant role in the ecosystem functionality of mountain landscapes and nearby lowlands by providing important hydrological and ecological controls. For example, alpine wetlands mitigate flooding, minimize storm damage, provide water for consumption and irrigation, and support important ecological habitats (Aber et al. 2012).

Alpine vegetation often experiences a shorter growing season than those located in lowlands, which influences plant phenology. As a result, vegetation in the alpine zone experiences slow growth rates and extended life cycles (Pauli et al. 1999). Thus, mountain regions have high plant biodiversity, but exhibit distinct ecotones with sharp changes from landscapes dominated by vegetation and soil, to those by snow and ice (Beniston, 2006). Mountain vegetation is also often endemic, due to isolation and a lack of competition at higher elevations (Beniston, 2006). Therefore, flora located within the alpine zone is at the edge of its environmental tolerance and is vulnerable to any small changes in the abiotic processes governing them, particularly climate (Cannone et al. 2007). Because of slow growth rates and longer life cycles of species (Pauli et al. 1999), alpine vegetation is expected to be more sensitive to long term changes in climate and less sensitive to temporary climate fluctuations (Gottfried et al. 1998; Theurillat & Guisan, 2001). This complex relationship between vegetation and climate in mountains has been proven by a shift in community composition over the last 50 years (Cannone et al. 2007). From 1953 to 2003 there has been an upward migration of tree and woody shrubs by 120 – 340 m (Kullman, 2002), and 40 – 50 m for alpine and nival plant species (Grabherr et al. 1994; Walther et al. 2005). In the elevation band of 2230 to 2400 m.a.s.l. there has been a 33 % increase of shrubs, a 31 % decrease in grasslands and a 7 % decrease in wetlands (Cannone et al. 2007).

1.5 Knowledge Gaps

There are numerous anthropogenically induced issues facing mountain regions that require increased understanding of these complex environments. Population growth into alpine areas has increased the accessibility to previously untouched landscapes, and has provided the opportunity for agriculture, forestry, mining, and hydroelectric developments. The impacts associated with these changes, coupled with uncertainties regarding climate change have allowed forest disturbance to occur and increase wildfire risk, insect infestation, and disease (Fang et al. 2013). Due to anticipated risks in future drought and flooding, increased hydrologic knowledge and understanding within alpine catchments is required (Bales et al. 2006). Therefore, the literature has identified a greater understanding of the processes that regulate the partitioning of energy and water fluxes into and out of these complex systems as a leading hydrological need in mountain areas worldwide (Bales et al. 2006).

Topographic aspect is an important control in alpine ecosystems because it regulates the amount of incident solar radiation that is able to reach the surface (Chen et al. 2016). Fluctuations in radiation during the day from shading influence the local microclimate and its hydrothermal processes like evapotranspiration (ET) (Badano et al. 2005; Benniea et al. 2008). Therefore, light availability and the radiation balance are important abiotic factors that limit plant growth worldwide, yet little is known about their role, or relative importance within the alpine zone (Larcher, 2006; Onipchenko et al. 2001). Although ET has been extensively researched, it and other physical processes remain poorly characterized within a broad range of different wetland types (Souch et al. 1996). ET measurements are also highly variable within different vegetation and climate zones, so wetland types that have been extensively monitored are not fully comparable to those that are less understood (Campbell & Williamson, 1997).

Wetlands are one of the largest unknown ecosystems in regard to understanding future carbon budgets (Sulman et al. 2009). Relatively few studies have been conducted on carbon cycling in alpine wetlands, and as a result, these systems remain some of the least understood (Wickland, 2001; Cao et al. 2017). Although it has been found that under future climate change scenarios wetlands may shift from sink to source, minimal research has been done on determining carbon source/sink strength in alpine wetlands and its controlling variables (Cao et al. 2017). Therefore, further research is required to broaden our knowledge on ecosystem carbon exchange, its controlling mechanisms, and on carbon uptake in mountain wetlands.

1.6 Research Objectives

The overall research objective of this thesis is to enhance the literature on microclimates within complex terrain. This thesis will focus on a heavily shaded wetland site in the Kananaskis Valley of the Canadian Rocky Mountains. This is the first of a four-chapter manuscript style thesis, which began by providing a detailed background on existing literature and the rationale for this study. The second chapter (manuscript 1) will focus on the spatial and temporal patterns of shade and how that influences incident solar radiation and components of the surface energy budget; while, the third chapter (manuscript 2) will investigate 2018 seasonal flux patterns (water and carbon) and the influence of shade on daily fluxes. Chapter 4 will provide a summary of the study and address limitations that were encountered.

Chapter 2: Manuscript 1: Horizon shade reduces energy fluxes and influences the microclimate of a subalpine wetland in the Canadian Rocky Mountains.

2.1 Introduction

Earth's boundary layer energy fluxes control many hydrological processes. Within mountain landscapes, the partitioning of energy directly influences regional hydrology, including: snowpack formation, the timing of snowmelt, and the availability of water for soil and vegetation use throughout the growing season (Turnipseed et al. 2002). The closed energy budget for mountain ecosystems is expressed as,

$$Q^* = Q_e + Q_h + Q_g \tag{1}$$

where the net available energy (Q^*) is partitioned between the turbulent fluxes of latent (Q_e) and sensible (Q_h) heat, and the conductive flux of ground heat (Q_g). The energy budget is important at the surface to help control moisture conditions (Knowles et al. 2015). The energy budget is often negative during the winter months and overnight, and is characterized by cool temperatures that may reach below 0°C and permit water to freeze. However, positive net energy during the summer drives warming surface temperatures and promotes the transfer of energy from the surface to the lower atmosphere.

Shortwave ($K\downarrow$) downwelling radiative fluxes is part of the surface radiation balance and is important to consider when evaluating snow melt and mountain water storage. The radiation budget at any location on the Earth's surface is defined as,

$$Q^* = K^* + L^* = K\downarrow - K\uparrow + L\downarrow - L\uparrow \tag{2}$$

where Q^*, K^*, and L^* are net all-wave, shortwave, and longwave radiation, respectively. K^* is defined by incident shortwave radiation ($K\downarrow$) and reflected (outgoing) shortwave radiation ($K\uparrow$), while L^* represents incident longwave radiation ($L\downarrow$) and reflected (outgoing) longwave radiation ($L\uparrow$). $K\downarrow$ generally has low spatial variability over small areas, except for regions with complex terrain (Oke, 1987; Ma et al. 2016). Direct solar radiation received at the Earth's surface is a function of latitude, time of day and year. However, topography is another important variable to

7

consider, especially in mountain landscapes, where it may dramatically change the amount of radiation that reaches the surface during different daily and seasonal periods (Oke, 1987; Spokas & Forcella, 2006; Ebrahimi & Marshall, 2016).
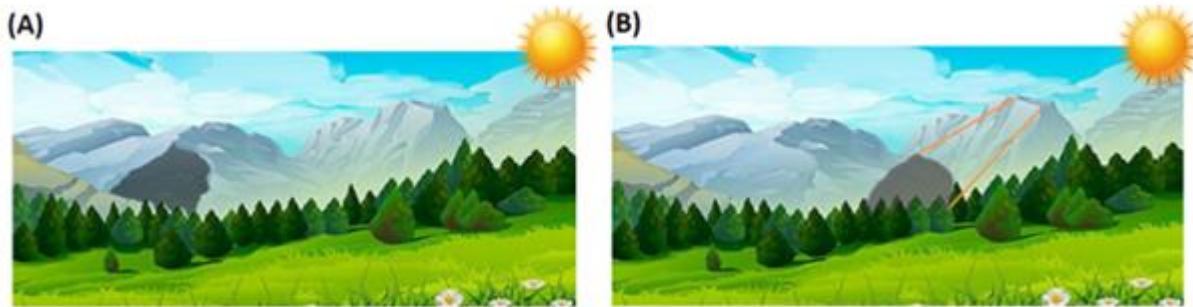
Figure 2-1: Conceptual model of a (A) self and (B) horizon shadows in an alpine environment.

In mountain regions, topographical features like slope, aspect, and land surface exposure have a direct relationship with the surface energy balance and may lead to the establishment of localized microclimate conditions. Shadows are common features in mountains where summits, ridges, and headwalls act as barriers to light. Different types of shadows have been described in alpine regions. A horizon shadow (Figure 2-1B) is a condition when the land surface is shaded from surrounding topography (i.e. a summit, headwall, or ridge), because it is below the local horizon and blocked from direct-beam irradiance (Essery & Marks, 2007; Marsh et al. 2012). Self shadows are a subclass of horizon shadows and are more associated with aspect (Figure 2-1A) (Marsh et al. 2012). Under self-shadow conditions, the shadow is cast by a terrain feature onto itself when the slope is facing away from the sun (Marsh et al. 2012). Both shadow types promote large differences in K↓ and impact the surface energy budget over small surface areas (Marsh et al. 2012). The result is that microclimates are established in areas of complex terrain, because land surfaces are constantly being cycled in and out of shadows that results in a lower daily radiative input compared to surrounding non-shadowed regions. Microclimates that result from horizon shadows are important within alpine systems, through regulating temperature, photosynthesis, and vegetation phenology (Pomeroy et al. 2003; Dymond, 2002). For example, studies in the Scandinavian Mountains of Northern Europe have found that complex terrain decreases average annual temperatures by 2 – 6°C (Ackerly, 2010; Scherrer & Korner, 2011; Graae et al. 2012; Lenoir et al. 2013).

Alpine wetlands were chosen for this study because they are important features within these landscapes and provide significant hydrological and ecological services by mitigating floods, minimizing storm damage, providing water for downstream communities, and supporting important habitats (Aber et al. 2012). While we know that shadows influence temperatures and plants, little to no work has been done on the direct impact of shadows on the surface energy balance and how those impacts affect local hydrology (Larcher, 2006; Onipchenko et al. 2001). Historically, research on the relationship between energy and water fluxes in mountain ecosystems has observed snow melt processes during transitional periods of snow and ice cover (Pluss & Mazzoni, 1994; Marks et al. 2008; Ma et al. 2016). Therefore, a greater understanding of the processes that regulate the partitioning of energy and water into and out of alpine wetlands during the growing season is a leading hydrological need in mountain areas worldwide (Bales et al. 2006). As a result, the goal of this paper is to quantify the influence of complex terrain on the energy budget within isolated microclimates, using a sub-alpine wetland as an example given the strong controls of radiation on the mass and energy fluxes in a non-moisture limited system. The objectives are to: (1) partition the energy budget of a sub-alpine wetland; and (2) evaluate the impact of horizon shade on solar radiation and components of the energy budget.

2.2 Study Site

The study was conducted at a wetland on Fortress Mountain (50.82°N, 115.21°W), a privately-owned alpine ski resort in the Kananaskis Valley, which marks the front range of the Canadian Rocky Mountains. Fortress Mountain is located 30 km South of Canmore and 80 km West of Calgary, Alberta (Figure 2A). A tall steep headwall of approximately 500 m in height marks the southern boundary, an ephemeral tarn is located 200 m to the North, while Canadian and Fortress Ridges (~150 m) are the drainage divides 500 m to East and 1.7 km to the West (Figure 2-2C). The alpine wetland (2,083 m a.s.l.) from here on referred to as Bonsai, falls within the marsh meadow with freshwater classification of Rocky Mountain wetlands (Windell et al. 1986), is located directly beneath the headwall and covers approximately 1 ha (Figure 2-2C). The wetland is mostly flat, with a moderate increasing slope of 6 degrees resulting from a 3 m change in elevation over 50 m in horizontal distance from the tarn to the talus slopes. The talus slopes rise approximately 200 m above Bonsai and extends from the wetland to the base of the headwall. The headwall to the South and ridge to the East of the wetland provide a topographic barrier that is

believed to influence the ecohydrological characteristics of the site (Christensen, 2017). The wetland is shaded for extended periods of time during the day, but the total daily duration of shade shifts from spring (longer) to summer (shorter) and fall (longer). This shading has created a microclimate that promotes a thick snowpack, long snow-covered season, an extended spring melt, and a constrained growing period compared to other more exposed areas on Fortress Mountain (Figure 2-3).
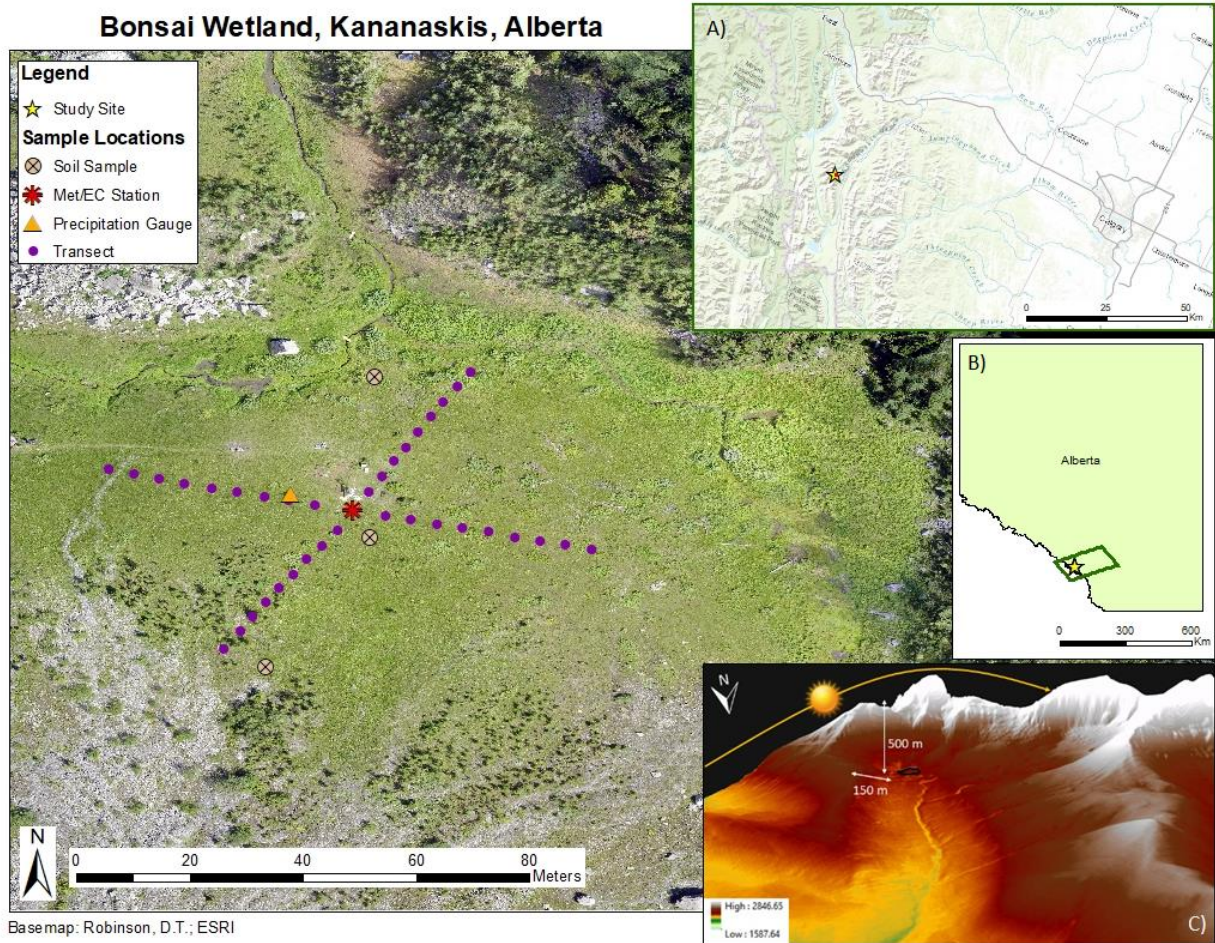
Figure 2-2: Site map Bonsai wetland, showing the location of equipment/sampling, its location in the province of Alberta and the Eastern Rockies (A/B), and LIDAR imagery of the basin with daily sun path and topographic boundary elevations (C).

Figure 2-3: Images of the seasonal evolution of Bonsai during A) *Snow Cover***, B)** *Snow Melt***, C)** *Green Up***, and D)** *Peak Growing Season***. Images were taken during the 2018 field campaign on A) June 8th, B) June 18th, C) July 6th, D) July 26th.**

Surface water from two creeks meet at a confluence in the North-Central section of the wetland and drain into a tarn which feeds Galatea Creek, and later, the Kananaskis River (a tributary to the Bow River). The two main stream branches follow the East and West boundaries of the wetland and are fed by springs emerging from talus deposits (Christensen, 2017). The Eastern stream floods during spring melt and water pools above the ground surface for several weeks in the North-East corner. Following spring melt, the stream in the West flows continuously during the growing season, but the stream in the East often dries by midseason.

Climate conditions within the Kananaskis Valley are representative of continental air masses where winters are generally long and cold, with an average temperature of -15 °C from January to March (DeBeer & Pomeroy, 2009). The average annual precipitation is approximately 900 mm in the valleys and mid-elevations but increases to 1140 mm above the treeline (Storr, 1967). Historically, 65 to 70 % of average precipitation occurs as snowfall (DeBeer & Pomeroy, 2009). Due to cold temperatures and high snowfall, snow cover persists in the basin from November to June (Marsh et al. 2012) with a melt period that lasts from April until July (DeBeer & Pomeroy, 2009). The closest Environment and Climate Change Canada (ECCC) weather station (ID 3053600) with 30+ years of climate records is located 28 km North of the study site at an

elevation of 1,391 m a.s.l. (51.03 N, 115.03 W). Average daily temperatures from June to August are 11.4 °C, 14.5 °C, and 13.8 °C, respectively, with an annual minimum of -6.2 °C in December and maximum of 14.5 °C in July (Figure 2-4). Average annual precipitation is 639.3 mm, with 119.4 mm, 64.9 mm, and 70.8 mm falling over the summer months of June, July, and August (Figure 2-4).
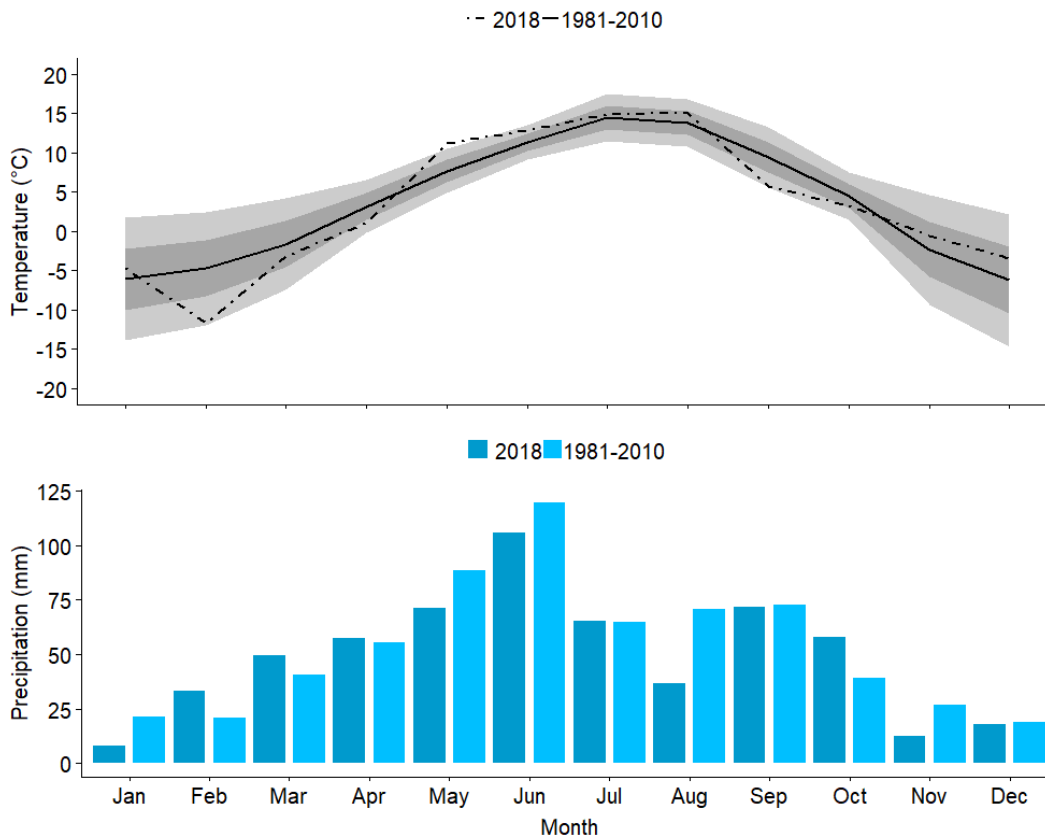
Figure 2-4: Environment and Climate Change Canada 30-year climate normals (1981-2010) weather station (ID 3053600) located 28 km North of the study site at an elevation of 1,391 m a.s.l. in the Kananaskis Valley (51.03 N, 115.03 W). One and two Standard deviations outlined in temperature.

Soil and vegetation conditions differ across the wetland in a North to South gradient (stream confluence to the headwall). Near the stream, the wetland is characterised by a thin layer of pervious well sorted sand above a semi-pervious layer of very fine silt (Table 2-1). Well sorted soils near the stream in the north of the wetland encourage the establishment of *Erigeron caespitosus*, of the family *Asteraceae*, native to Western Canada and the Rocky Mountains (Figure 2-5). The centre of the wetland has the highest percent of organic matter (LOI) and is defined by silt and clay that is moist and plastic but not fully saturated (Christensen, 2017). The middle of

the study area is mostly covered by shade tolerant species like *Equisetum, Salix, Castilleja raupii* and Litter (Figure 2-5). Litter is highest here because of *Salix*, a broadleaf shrub that loses its leaves. Finally, brown moss is the dominant groundcover type nearest to the headwall. Across the wetland, soil begins to surpass field capacity at 2 m and becomes increasingly saturated with depth (Christensen, 2017).
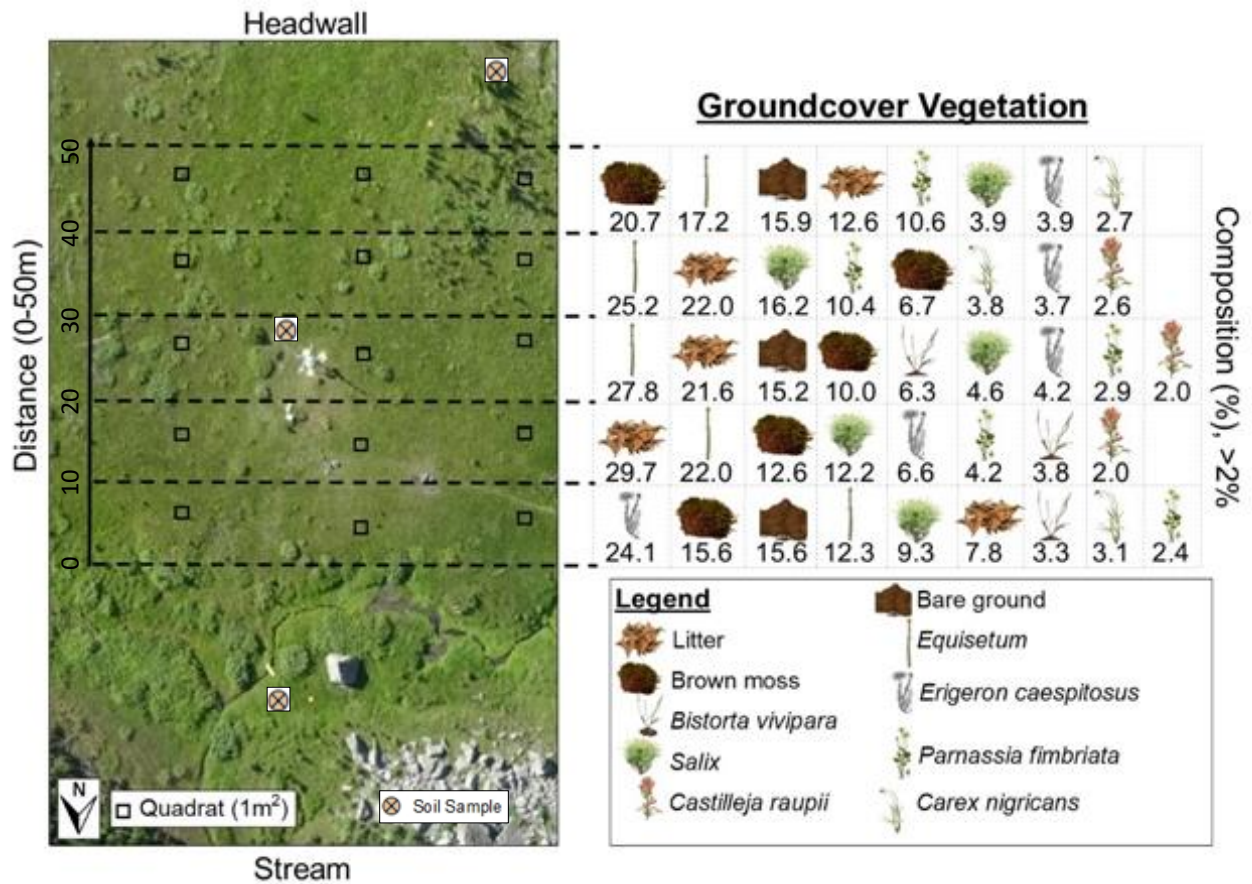
Figure 2-5: Groundcover and vegetation survey results along 3 transects from the stream confluence to headwall (N→S).

Table 2-1: Soil characteristics from North to South (N→S) along an increasing elevational gradient, and exposure to shade.

	North		Middle		South
	Stream Confluence (0-15.5cm)	Stream Confluence (15.5-31cm)	Tower (0-9.5cm)	Tower (9.5-29.5cm)	Headwall (0-15cm)
Avg Ksat (cm/s)	$1*10^{-1}$	$5*10^{-5}$	$7*10^{-2}$	$9*10^{-5}$	$1*10^{-1}$
Avg Ksat (m/day)	95.00	0.04	59.16	0.08	107.61
BD (g/cm³)	1.64	1.50	1.10	1.12	0.49
LOI (%)	5.22	4.91	10.20	6.80	6.92
Permeability	Pervious	Semi-pervious	Semi-pervious	Semi-pervious	Pervious
Texture	Silt Loam	Silt Loam	Loamy Sand	Sandy Loam	Loamy Sand

2.3 Materials & Methods

2.3.1 Soil Sampling and Analyses

Three intact soil cores were removed from the ground with a 3-inch PVC pipe to a depth of ~30 cm in the wetland and ~15 cm near the talus slope. Care was taken to not compress the organic layer by cutting along the edges of the pipe. Loose soil samples were collected with a hand auger to a depth of 1 m in the wetland and 30 cm near the talus slope. The samples were separated into 10 cm intervals and stored in a cooler for transportation until analyses could be conducted. Once in the lab, soil samples were prepared and processed for saturated hydraulic conductivity (K_{sat}) (Freeze & Cherry, 1979) , Bulk Density (BD) and Loss on Ignition (LOI) following standard protocols (Dean, 1974), but oven dried at 80°C during BD to minimize loss of organic matter (Freeze & Cherry, 1979). The intact samples within PVC pipe were separated into two depths representing a surface layer (>15 cm) and a deeper layer (15-30 cm); however, due to measurement error, one core was divided into a surface layer of 10 cm and a lower layer of 10-30 cm. The loose (bulk) samples were dried in an oven at 100°C for 72 hours and then broken down with a pestle and mortar and put through a 2 mm sieve in preparation for soil texture. A Horiba LA-950 V2 Particle Size Analyzer was used to sort the samples as sand, silt, or clay. The Krumbein Phi-Scale

was used for soil texture classification, where particle size was determined by: sand (62.5 um – 2 mm), silt (3.90625 – 62.5 um), and clay (< 3.90625 um).

2.3.2 Vegetation

A vegetation survey was conducted on August 14th, 2018 by the Rooney Lab, Department of Biology, University of Waterloo (Rooney et al. 2018, unpublished). Three transects were placed in parallel lines in a North to South (Stream to Headwall) direction across the wetland (Figure 2-5). Each transect was 50 m in length and was separated by 25 m. A 1 m quadrat was placed every 10 m along each transect and percentage of groundcover vegetation was estimated within each. Seedlings that were too small to identify were not included. Each transect was completed twice and averaged to ensure a representative sample.

2.3.3 Meteorological Data

A meteorological tower was installed in the approximate centre of the wetland and instrumented with equipment to measure meteorological variables. Wind speed was measured at a height of 3.8 m (R.M. Young 05103 – 10A anemometer, Traverse City, Michigan, USA), while net radiation (NR Lite, Kipp and Zonen, Delft, Netherlands) and photosynthetically active radiation (Li-Cor 2319, Lincoln, Nebraska, USA) were measured at 3.05 m. Air temperature (T_a) and relative humidity (RH) were measured at 3.4 m (Vaisala HMP 155, Helsinki, Finland). Two soil heat flux plates (Husk Flux Thermal Sensor HFP01, Delft, Netherlands), were placed under the soil surface at a depth of 5 cm to measure an average ground heat flux. Two ECH2O EC – 5 sensors (Meter Group, Hopkins, Washington, USA) measured the average soil moisture at 10 cm depths. Soil temperature (T_s) was measured at 3 depths (2, 5, & 10 cm) with Soil Thermistors (Li-Cor 7900 – 180; Lincoln, Nebraska, USA). Meteorological equipment was installed from June 7th to September 10th, to monitor the 2018 growing season. Data was recorded on a 9210XLite Logger (Sutron, Stirling, Virginia, USA), sampled every 10 seconds and averaged every 30 minutes. Precipitation was measured at a nearby meteorological station, approximately 350 m north, at the same elevation, in a clearing on the opposite side of Bonsai Lake by a tipping bucket rain gauge data logger (Hoskin Scientific, Burnaby, British Columbia, Canada).

2.3.4 Eddy Covariance Measurements

The latent (Q_e) and sensible (Q_h) energy fluxes were measured with Eddy Covariance (EC) instrumentation during the same time period as the meteorological data. EC measurements at Bonsai were collected with a three-dimensional sonic anemometer (CSAT3; Campbell Scientific Inc., Logan, Utah, USA) and an open-path infrared CO_2 / H_2O gas analyzer (IRGA) (LI-7500, LI-COR Inc., Lincoln, Nebraska, USA) installed at a height of 3 m above the surface on the meteorological tower. The EC system was calibrated to sample fluxes at a frequency of 10 Hz with averages calculated and recorded on a data logger (CR1000; Campbell Scientific Inc., Logan, Utah, USA) at 30-minute intervals.

EC processing followed standard protocols found in the literature and was partitioned using REddyProc in Rstudio (RStudio Team, 2016). To ensure quality and reliable EC data, it was corrected to ensure turbulent mixing, functioning instrumentation, and that data being used was sourced from within the wetland only (Petrone et al. 2015; Rocha & Goulden, 2009). EC data was quality controlled to remove outliers greater than two standard deviations of the mean (Papale et al. 2006) and was gap filled based on a 14-day mean moving window (Falge et al. 2001). The 30-minute average fluxes were filtered for periods of low atmospheric turbulence and later corrected for density and sensor seperation within the flux footprint. Final corrections were incorporated from Petrone et al. (2001), Wilson et al. (2002), and Brown et al. (2010) and are listed in Appendix 1.

2.3.5 Hill shade Model

Coordinates from Bonsai tower were input into www.suncalc.org (Hoffmann, 2018), a free publicly available website tool that provides solar data for selected dates and times across the globe. This tool provided the azimuth, altitude, and shadow length every 15-minutes for clear-sky days from June 7th to September 10th. Clear sky days were selected based on daily field observations while at site and through near perfect daily K↓ bell-curve plots. All records were downloaded and compiled into a single table, negative altitude values (time when the sun is below the horizon) were removed to avoid error in the hill shade calculation. These data, along with a Digital Elevation Model (DEM), were used as input into a hill shade model in ArcMap (v10.6). First, hill shade rasters were created via the hill shade tool and clipped to the study area. Each hill shade raster was reclassified to set shadows to 0 and all other values to 1. The raster calculator

was used to create one hillshade raster that represented the sum of all the rasters for each day. Each value for the summed hill shade raster was converted to total hours shaded for each clear sky day, using,

$$\text{Hours shaded} = \frac{(\text{Shade value}) * 15 \text{ minutes}}{60 \text{ minutes/hour}} \qquad (3)$$

where shade value was the value of the summed hill shade raster.

2.3.6 Solar Radiation Model

To calculate daily K↓ across the study site, the Area Solar Radiation tool was used in ArcMap (v10.6). This tool derives incoming K↓ from a raster surface based on the amount that would be intercepted from surrounding topography (via the DEM). Only daylight hours were input to the model, to ensure that the results would be comparable to the Hill shade model. The output was then run through the "int" tool to convert the value of each raster to an integer by means of truncation. Next, "extract by mask" was used to isolate the wetland values from the rest of the basin. Final K↓ values for the wetland were then overlain on top of each other to compare hours shaded and K↓. To quantify intercepted radiation, the solar radiation model was run for a ridge located 2.4 km North of Bonsai with no topographic barrier to block K↓. K↓ at Bonsai was then subtracted from K↓ at the ridge and the difference was assumed to approximate the amount of radiation directly intercepted by the headwall. To interpolate observed K↓, PAR values were converted to W/m^2 by multiplying by 0.219 as indicated in the Plant Growth Chamber Handbook (McFarlane & Sager, 1998) that was adapted from Thimijan & Heins (1983), then multiplied by 2 to represent the full spectrum of K↓.

2.3.7 Statistical Analysis

All statistical analyses were performed and summarized with R packages dplyr, reshape2, tidyr, and forcats then illustrated with ggplot2 in RStudio (RStudio Team, 2016). Before any analysis was conducted, all data was assessed for normality with a Shapiro-Wilks normality test. The Shapiro-Wilks test concluded that all data was normaly distributed ($p > 0.05$), with the exception of the output from the hill shade model. The sample size from the solar radiation model was too large to compute with a Shapiro-Wilks test ($n > 5,000$) so it was analyzed with a Quantile-Quantile

17

(Q-Q) plot. The Q-Q plot indicated that daily K↓ was non-normal so non-parametric testing was used to analyze the hillshade and solar radiation models.

To ensure that shade was an appropriate metric to use in a statistical analysis, it was first compared to the intercepted radiation by the headwall. It was found that intercepted K↓ increased alongside shade as the season progressed, indicating that increased shade reduced K↓. Since more shade resulted in greater K↓ interception, its influence on components of the surface energy budget was important to understand (Q^*, Q_e, Q_h, and K↓). A linear regression model was used to understand the influence of shade (independent variable) on components of the energy budget (dependent variables). Since the ouput from the hill shade model was the independent variable, parametric testing was acceptable to use in this section of the study. To help isolate shade in the statistical analysis, the data was divided based into the periods of *Stable Shade* with constant average daily shade (June 7th to July 30th) and *Dynamic Shade* with increasing average daily shade (July 31st to September 10th).

2.4 Results

2.4.1 Climatic Conditions

Average daily air temperature during the study period (June 7th to September 10th) was 9 °C (±4.1), with a daily maximum of 18.6 °C on August 10th and a daily minimum of 0.8 °C on June 11th (Figure 2-6). The ground surface remained frozen until June 20th when T_s (2 cm) quickly thawed over three days, increasing in temperature from -0.3 °C to 7.4 °C (Figure 2-6a). This thaw period in the soil profile coincided with the time when the ground surface near the tower started to become snow free. Monthly air temperatures during the study period fell within 2 standard deviations (except for May) of the ECCC (ID 3053600) 30-year climate normals for the region (1981-2010), indicating that this was a normal and representative growing season based on temperature (Figure 2-4). During the study period, temperatures remained within the higher end of the expected range, other than in September when it was cooler than the 30-year average (Figure 2-4). Historically, average monthly temperatures at the ECCC station are 11.4 °C (±1.1), 14.5 °C (±1.5), 13.8 °C (±1.5), and 9.4 °C (±1.9) in June, July, August, and September (Figure 2-4). 2018 temperatures at the ECCC station were normally distributed as they fell within two standard deviations of the monthly climate normals with 12.9 °C, 14.9 °C, 15.1 °C, and 5.7 °C, respectively (Figure 2-4).

18
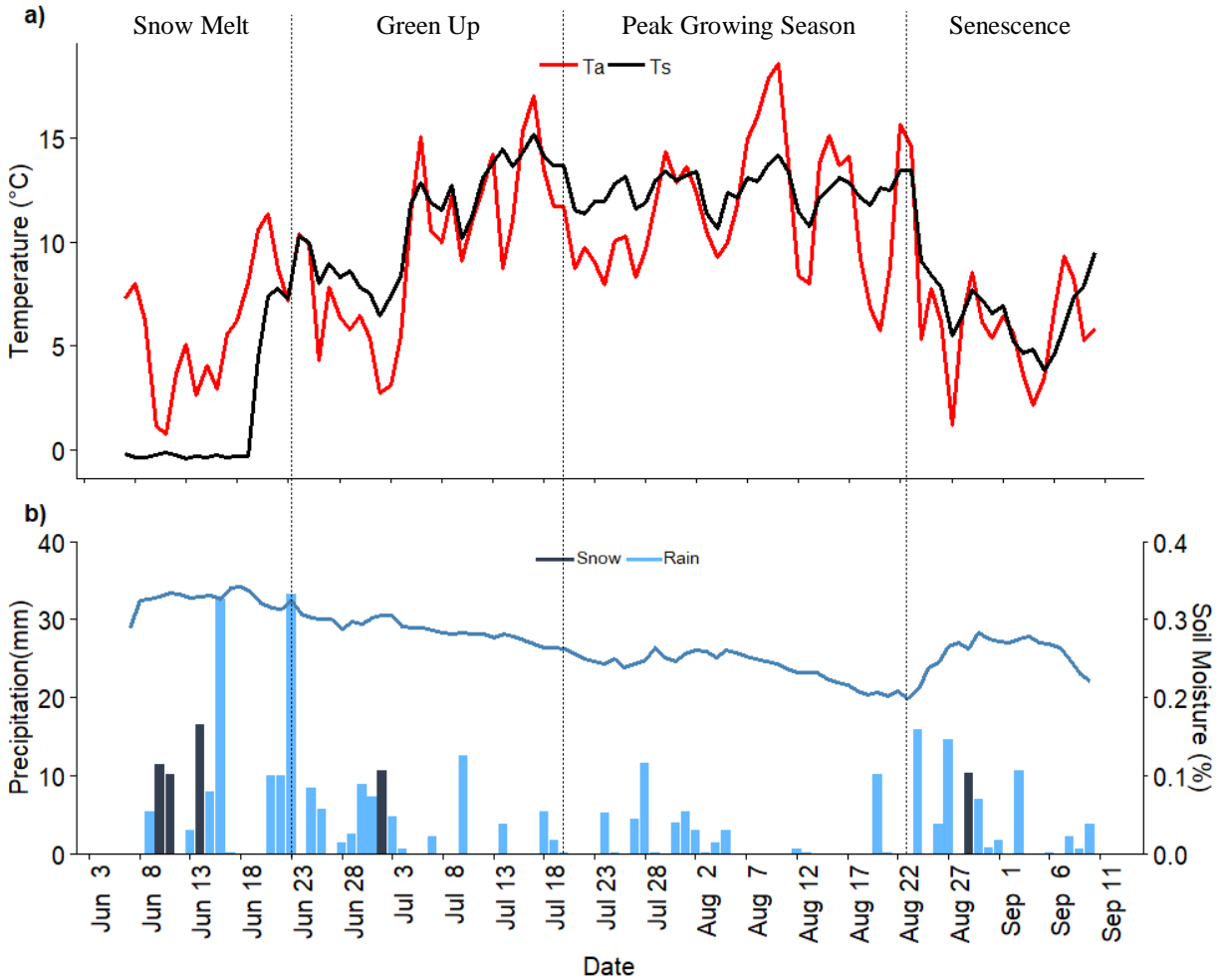
Figure 2-6: Climate trends over 2018 field season. a) air temperature (Ta) and surface soil temperature (Ts) at 2cm; b) precipitation defined by snow and rain, and soil moisture.

Historically, 65-70 % of total annual precipitation occurs as snowfall in the area, with 900 mm in the valley and mid-elevations to upwards of 1140 mm at the treeline (Storr, 1967; DeBeer & Pomeroy, 2009). Total precipitation for the wetland during the 2018 study period was 339 mm, close to the average cumulative rainfall amount of Marmot Basin (360 mm), 14 km North in the Kananaskis Range. The beginning of the study period had more frequent and intense precipitation events, with two days of rainfall surpassing 30 mm. High precipitation events occurred on June 16th and 23rd where each day received approximately 33 mm (Figure 2-6b). The basin was also heavily influenced by snowfall at the start of the growing season, with the last event captured through a time lapse camera on July 2nd (Figure 2-6b). Cumulative precipitation during the months of June, July, August, and September 2018 was 49 mm less than the 30-year climate normal for the region. When comparing the individual months, only July and September received the normal

amount of precipitation, while the other months had less than the 30-year norm, thus making 2018 a drier summer.
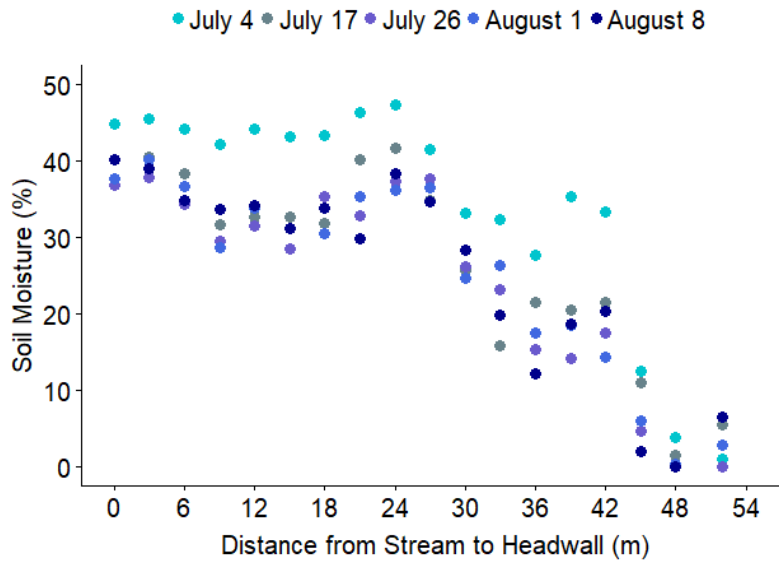
Figure 2-7: Spatial and temporal trend in soil moisture from the stream confluence (0 m) to the headwall (54 m).

In the middle of the wetland (20-30 m from the steam), the highest daily average soil volumetric moisture content (VMC) was recorded on June 18th (34.3 %), and lowest on August 23rd (20.0 %). VMC also decreased from the stream to the headwall. Figure 2-7 illustrates manual weekly VMC measurements taken along a North-South transect (in 3 m intervals) from the stream to the headwall. From 0-30 meters away from the stream, VMC was similar (38 % in July and 35% in August) with different spatial-temporal trends (Figure 2-7). In July, VMC was greatest near the stream and decreased toward the middle of the wetland; while in August the middle of the wetland had a higher VMC than the stream area (Figure 2-7). This was likely due to more pervious soil near the stream than the centre of the wetland (Table 2-1), and increased litterfall that has a greater ability to hold moisture (Figure 3-3). South of the tower, with increased proximity to the headwall, there was a rapid decrease in VMC because of coarser textured soil and gravel from the talus slopes (Table 2-1).

The remainder of the results section will compare seasonal trends during four time periods that were identified based on snowpack thickness and vegetation phenology observed visually throughout the study (Figure 2-3). These seasonal phases were: *Snow Melt* from June 7th to 23rd;

Green Up from June 24th to July 20th; *Peak Growing Season* from July 21st to August 23rd; and *Senescence* from August 24th until September 10th.

2.4.2 Energy Budget

Maximum daily Q* occurred on June 20th (196 W/m^2) (Figure 2-8a). Since most of the site remained snow covered on this date, evergreen vegetation that remained buried under the snow was not able utilize this maximum daily available energy (Q*-Q$_g$) in transpiration. When the site became entirely snow free in the middle of July, daily Q* was half the maximum amount (100 W/m^2) measured on June 20th. During day time hours (Q* > 10 W/m^2), Q* was highest during the *Green Up* period (236 W/m^2) and lowest during *Senescence* (78 W/m^2) (Table 2-2). K$\downarrow$ followed a similar trend as Q* through much of the *Peak Growing Season* but was higher during the *Snow Melt* period (Figure 2-8b), because the higher albedo of snow resulted in more K$\uparrow$.

Table 2 - 2: Average daytime (Q*>10 W/m^2) range of solar radiation (K$\downarrow$) and components of the energy balance during the clear sky days within each phase of the study period (W/m^2).

	K$\downarrow$	Q*	Q$_e$	Q$_h$	Q$_g$
Snow melt (June 7th – June 23rd)	336 ($\pm$35)	191 ($\pm$79)	93 ($\pm$34)	47 ($\pm$19)	26 ($\pm$41)
Green up (June 24th – July 20th)	331 ($\pm$34)	236 ($\pm$27)	129 ($\pm$24)	64 ($\pm$17)	38 ($\pm$7)
Peak Growing season (July 21st – Aug 23rd)	219 ($\pm$42)	151 ($\pm$35)	98 ($\pm$19)	32 ($\pm$11)	25 ($\pm$6)
Senescence (Aug 24th – Sept 10$^{th)}$	129 ($\pm$15)	78 ($\pm$18)	49 ($\pm$4)	17 ($\pm$10)	14 ($\pm$5)

When the entire site became snow free during *Peak Growing Season*, vegetation had 85 W/m^2 less per day than during *Green Up* to use in the transpiration processes (Table 2-2). Q$_e$ was the primary contributor to Q* over the entire study period; however, from July 16th onwards, Q$_e$ comprised a larger percentage of Q* because of decreases in Q$_h$ and Q$_g$. The Bowen ratio (ß) remained relatively constant over the study period but spiked from June 20th to June 30th with a daily average of 0.34 during snowmelt. During this time Q$_h$ and Q$_g$ utilized a greater proportion of Q* as snow temperature increased, and the soil began to thaw. Outside of the seasonal maximum, ß remained constant throughout *Green Up, Peak Growing Season,* and *Senescence* averaging approximately 0.1 per day.
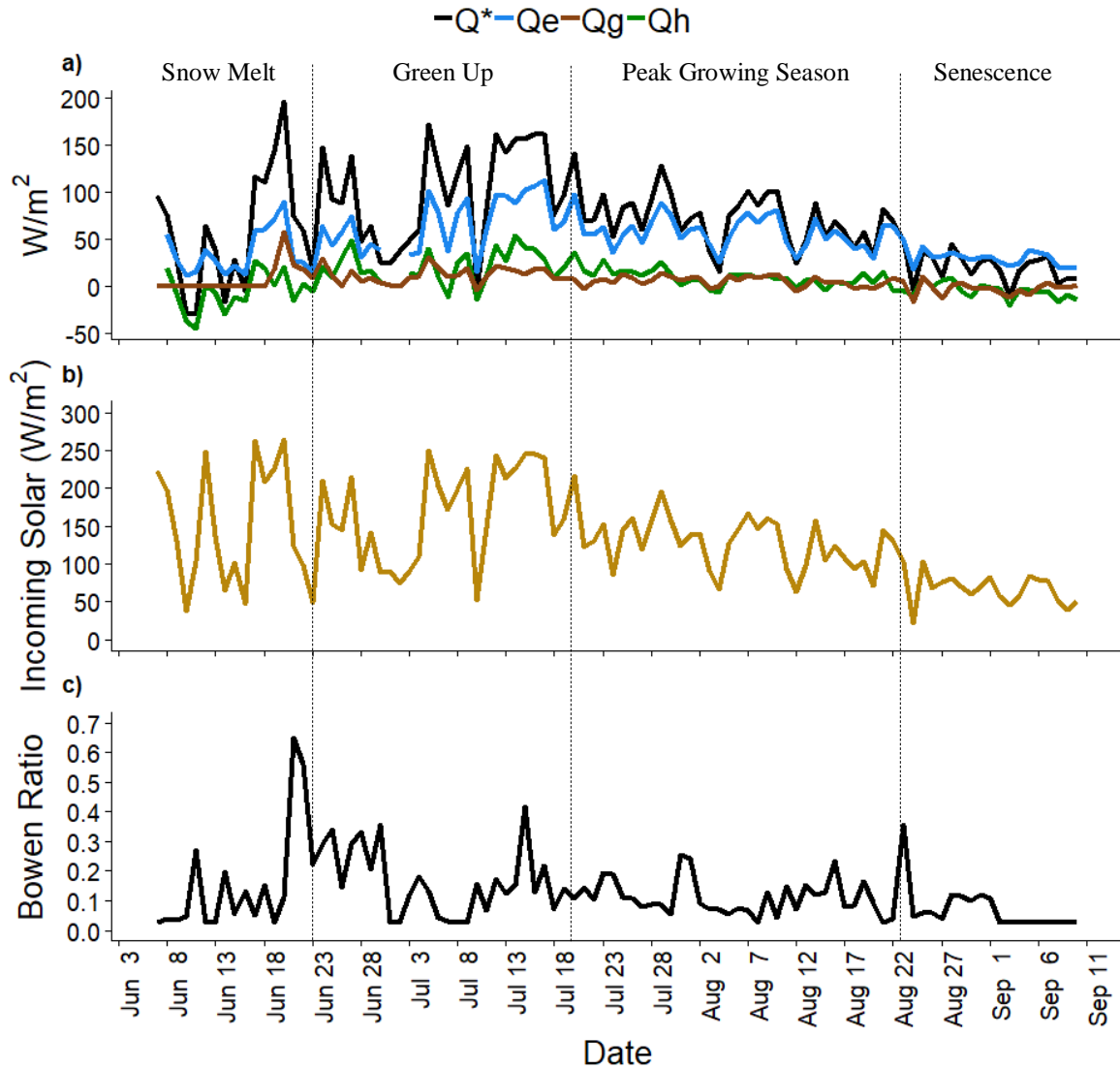
Figure 2-8: Daily average: (a) net radiation (Q*), sensible heat flux (Qh), latent heat flux (Qe), and ground heat flux (Qg) in W/m²; (b) Incoming Solar Radiation (K↓) (W/m²), & (c) Bowen Ratio (β) (Qh/Qe).

Maximum daily Q*, Q_e, Q_h, and Q_g occurred on June 20th, July 17th, July 14th, and June 19th, respectively (Figure 2-8a). The temporal difference in energy aligned with changes in maximum K↓ and shading. Maximum Q* occurred on June 20th, one day before the summer solstice when the sun was near its highest position in the sky. Because of the sun's higher altitude and azimuth during this time of year, there was increased sunlight hours and a lesser horizon shadow effect from the headwall onto the wetland. Q_g reached its maximum on June 19th when large contributions of energy were used to thaw the soil profile in patches of bare ground during

the period of peak snowmelt. Q_e and Q_h each reached their maximums in the middle of July, a normal time for peak vegetative productivity in alpine meadow and tundra ecosystems (Knowles et al. 2015; Cao et al. 2017; Millar et al. 2017).

2.4.3 Hill Shade

The wetland received an average of 2-3 ($\pm$1.1) hours of shade per day over most of the season with fluctuations in intensity and spatial distribution. At the beginning of the study (*Snow Melt* to *Green Up*), shade was more pronounced in the South-West (SW) corner and decreased in intensity along a diagonal gradient towards the North-East (NE) corner (Figure 2-9). At the same time, a ridge sheltered the East side of the basin resulting in increased shade East of the wetland and the tarn (Figure 2-9). July presented a similar spatial pattern in shade as June, but with increased intensity. By the end of the month, the horizon shadow established an average of 3-4 hours of shade per day through much of the wetland. Following July, shade continued to increase into August, strongly influenced by the headwall at the wetland. By the middle of August, shade no longer increased in a diagonal pattern across the wetland (SW$\rightarrow$NE), but rather straight from the headwall to the stream (S$\rightarrow$N) (Figure 2-9). This change to the spatial pattern covered a larger portion of the wetland, resulting in a rapid increase in the hours of shade per day from the beginning to the end of the month. From August 6th to the 26th, the site transitioned from 2.1 to 5.0 average hours of shade per day.

Table 2 - 3: Spatial and temporal variability in hours of shade per day across the site, during the four study periods of 2018.

	North	South	East	West
Snow Melt (June 7th – June 23rd)	1.85 ($\pm$0.29)	1.75 ($\pm$0.18)	2.10 ($\pm$0.29)	2.15 ($\pm$0.14)
Green Up (June 24th – July 20th)	1.66 ($\pm$0.36)	2.23 ($\pm$0.31)	1.93 ($\pm$0.39)	2.36 ($\pm$0.39)
Peak Growing Season (July 21st – Aug 23rd)	2.23 ($\pm$0.48)	3.15 ($\pm$0.98)	2.54 ($\pm$0.47)	2.85 ($\pm$0.62)
Senescence (Aug 24th – Sept 10th)	3.33 ($\pm$0.58)	7.25 ($\pm$0.87)	4.75 ($\pm$1.30)	5.33 ($\pm$1.01)
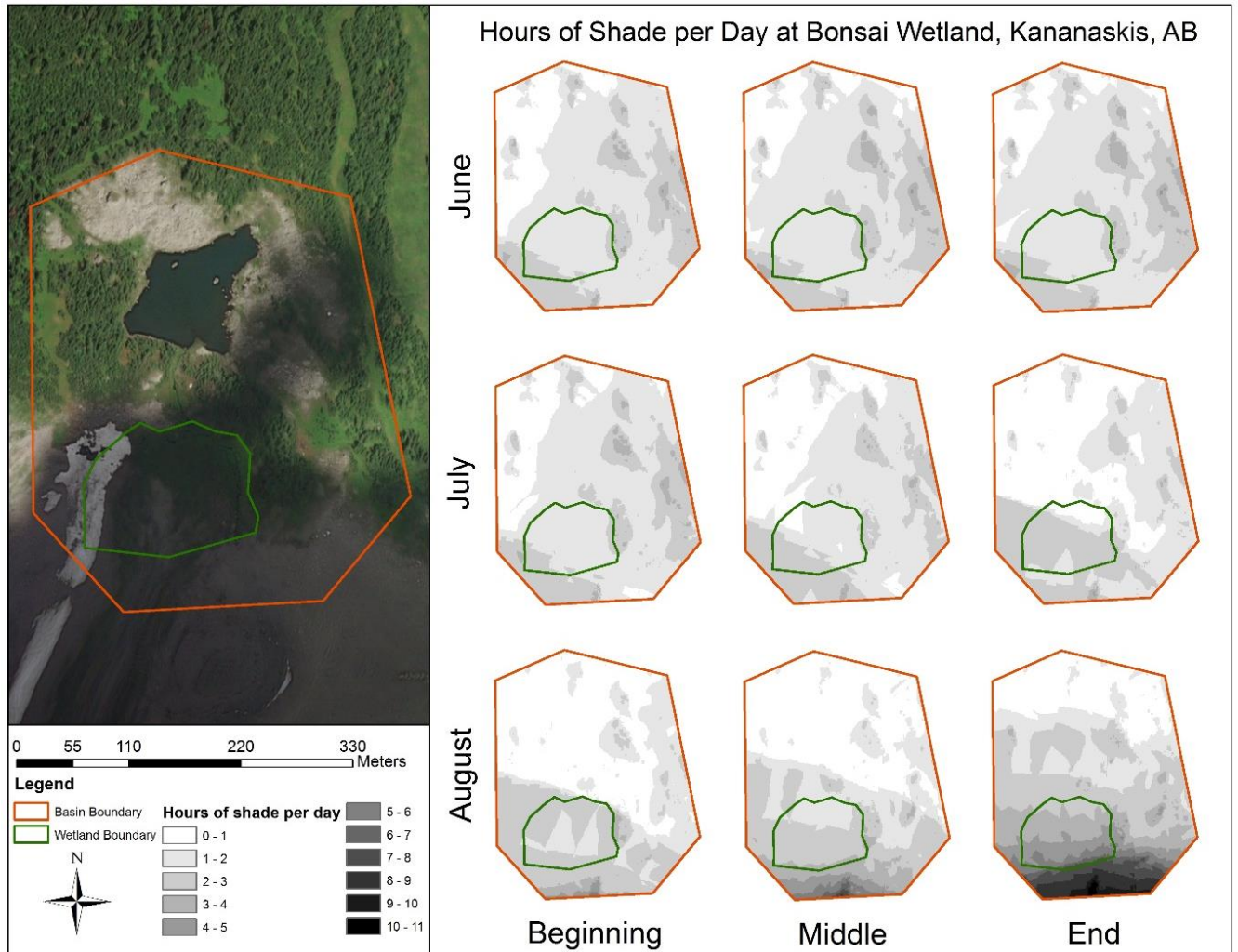
Figure 2-9: Hill shade model results for the beginning, middle, and end of each month during the 2018 observational period. Inset image illustrates the position and orientation of the site relative to the surround topography.

2.4.4 Shading Effects on Solar Radiation

Modelled K↓ slightly overestimated observed K↓ by 1 MJ until the middle of July and by > 5 MJ from mid-July to early September (Figure 2-10). The results showed that the average amount of intercepted radiation per day in *Snow Melt*, *Green up*, *Peak Growing Season*, and *Senescence* was 3.1, 3.4, 5.0 and 6.6 MJ; and that solar interception increased by 5.1 MJ from the beginning (June 17th) to the end of the study (September 10th) (Figure 2-10). This indicates that the horizon shadow effect became stronger as the season progressed, and more K↓ was intercepted prior to reaching the surface.
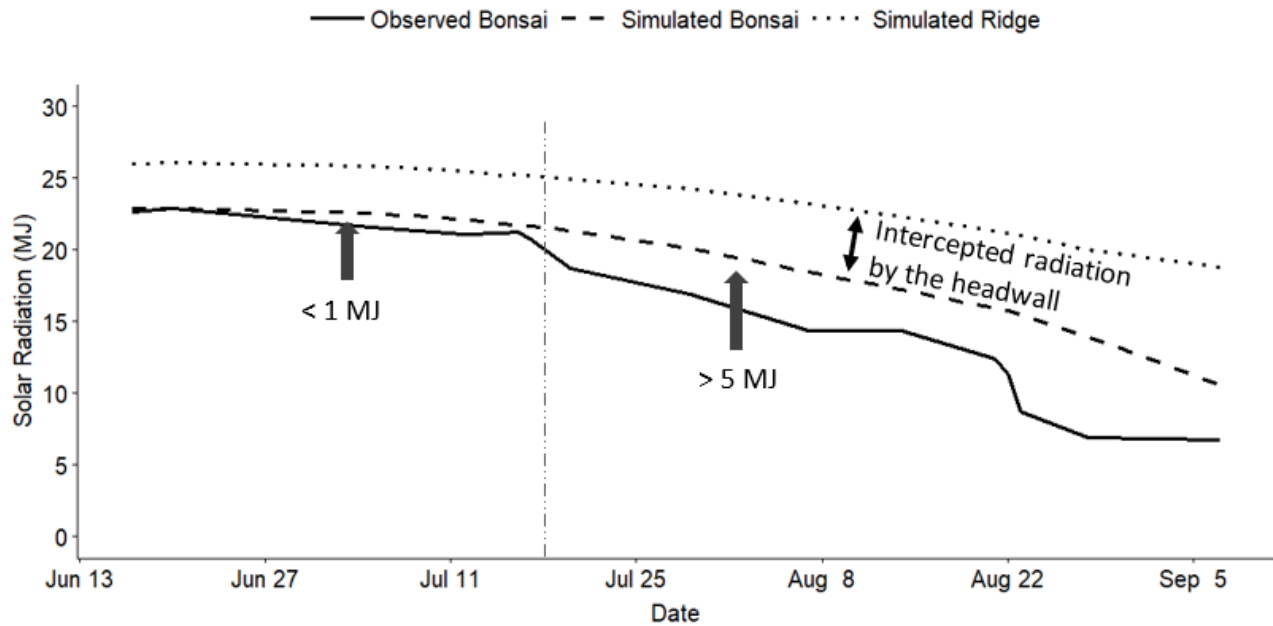
Figure 2-10: Comparison of total daily observed Solar Radiation at Bonsai, Simulated Solar Radiation at Bonsai, and Simulated Solar Radiation atop Fortress Ridge.

The relationship between cumulative daily K↓ and the average hours of shade per day was found to be statistically significant in *Dynamic Shade* but not in *Stable Shade* (Figure 2-11). A Kruskal-Wallis one-way analysis of variance found that there was a statistically significant difference ($p < 0.01$) from 1 to 11 hours of shade during *Dynamic Shade* (Figure 2-11). Further analysis with a Pairwise Wilcoxon Rank-Sum test indicated that certain hourly intervals in shade did result in similar cumulative daily K↓ (Table 2-4). The statistical analysis found that there was no significant difference in K↓ ($p < 0.05$) between 1 and 2 hours of shade per day, 5 and 11 hours of shade per day, and >7 and 11 hours of shade (Table 2-4). Therefore, across all seasons, days with this amount of shade found similar K↓.
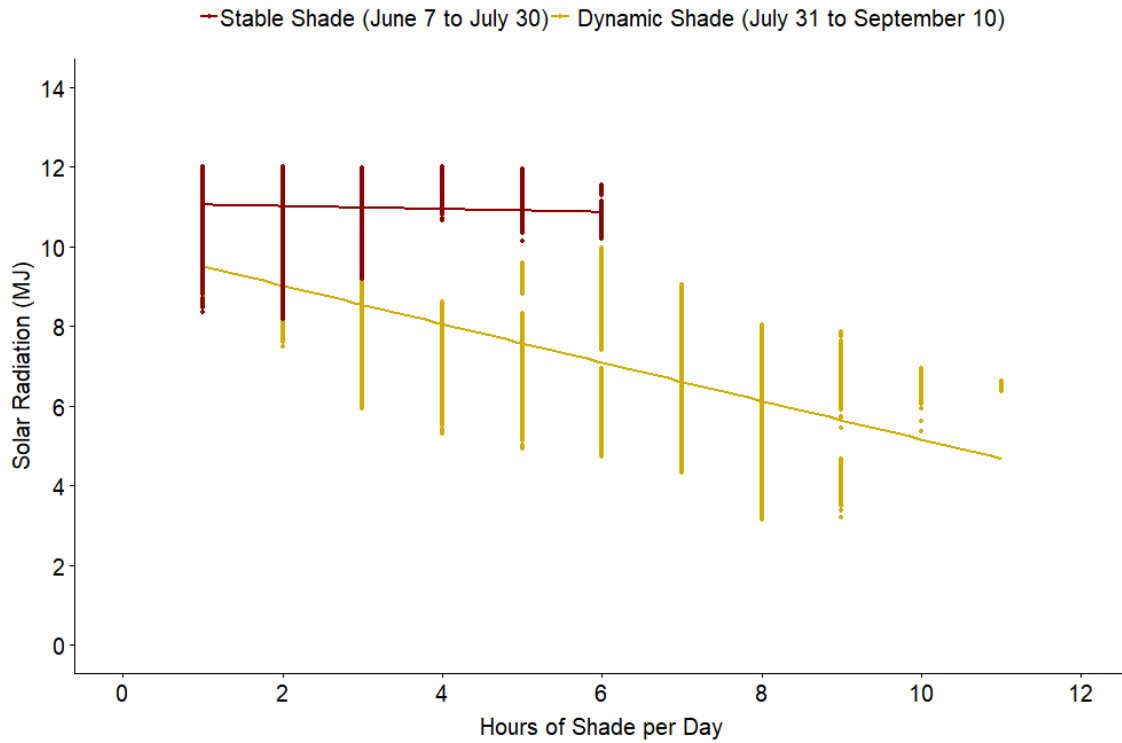
Figure 2-11: Relationship between the daily average clear sky solar radiation and hill shade model output of solar radiation during the periods of *Stable Shade* and *Dynamic Shade* at the Bonsai wetland, Fortress Mountain, Alberta, 2018.

Table 2-4: Wilcoxon rank-sum test with non-pooled standard deviation comparisons for solar radiation based on the average hours of shade per day during the period of increasing shade, Bonferonni P value adjustment method used. (ns not statistically significant, * <0.05, ** <0.001, * <0.0001, **** <0.00001)**

	1	2	3	4	5	6	7	8	9	10
2	ns									
3	****	****								
4	****	****	****							
5	****	****	****	****						
6	****	****	****	****	****					
7	****	****	****	****	****	****				
8	****	****	****	****	****	****	****			
9	****	****	****	****	****	****	****	****		
10	****	****	****	****	****	****	****	****	****	
11	****	****	****	*	ns	*	ns	ns	ns	ns

2.4.5 Energy Budget & Shade

Components of the energy budget had a statistically significant negative relationship with shade, indicating a more pronounced horizon shadow effect decreased available energy to the system. During *Dynamic Shade*, the regression model found that K↓ had a statistically significant negative relationship ($R^2 = 0.50$, $p < 0.05$) to hours of shade per day (Figure 2-12b). Therefore, every hour of shade per day in *Dynamic Shade*, reduced K↓ by 32 W/m^2 (y = -32.3 x +312.5). Q* also had a statistically significant ($R^2 = 0.55$, $p < 0.05$) relationship with hours of shade per day (Figure 2-12b), where each hourly interval of shade decreased Q* by 28 W/m^2 (y = -27.8 x +233.6). Finally, the regression model found that Q_e and Q_h also had a statistically significant relationship to the hours of shade per day in *Dynamic Shade* (Q_e: $R^2 = 0.63$, $p < 0.001$; Q_h: $R^2 = 0.29$, $p < 0.05$) (Figure 2-11b). For every hour of shade per day Q_e and Q_h were reduced by 18 W/m^2 (y = -17.9 x +149.4) and 6 W/m^2 (y = -5.9 x +48.4), respectively. Therefore, shade had a strong influence on the surface energy budget of Bonsai, where every hourly increase of shade during *Dynamic Shade* decreased each component of the energy budget (Q*, Q_e, and Q_h) by an average of 16 %. Therefore a 4 hour increase in shade would reduce the available energy by approximately 63 %.
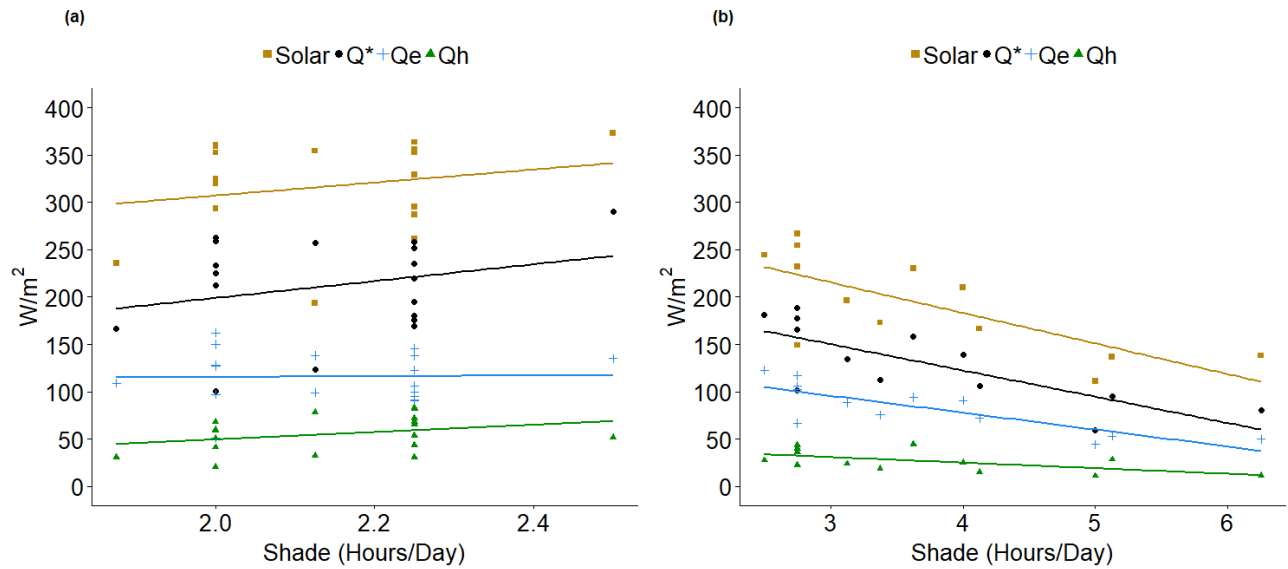
Figure 2-12: Relationship between hours of shade and Solar Radiation (Solar), Net Radiation (Q*), Latent Heat Flux (Q_h), and Sensible Heat Flux (Q_e) on clear sky days during the periods of (a) *Stable Shade*, and (b) *Dynamic Shade* at Bonsai wetland, Fortress Mountain, Alberta, 2018.

2.5 Discussion

2.5.1 Seasonal Subalpine Wetland Energy Partitioning

The timing of seasonal maximums in energy fluxes observed at our study site were consistent with those reported in literature on alpine energy balance (Ledrew, 1975; Konzelmann et al. 1997; Flerchinger et al. 2010; Knowles et al. 2014). However, there are inconsistent conclusions on energy balance contributions within the alpine meadow. For example, studies over the month of August at Niwot Ridge, Colorado found Q_h to be a greater contributor to the energy balance than Q_e, with average ß ranging from 1.30 to 1.37 (Ledrew, 1975; Knowles et al. 2014); while, the Swiss Alps found that the contribution of Q_e exceeded that of Q_h in August (ß=0.10-0.51) (Konzelmann et al. 1997). The difference in observations within mountain terrain has been attributed to variations in physical and climate features like aspect, slope, elevation, albedo, shading, sky view factor, and leaf area index. (Oliphant et al. 2003).

Konzelmann et al. (1997) found that Q_e comprised 65 % of the energy input of a meadow plateau (2220 m a.s.l.) and 85 % at a valley meadow (1,680m a.s.l.). From August 1st to the 27th the corresponding ß in their study was 0.51 and 0.1 at the plateau and valley, respectively (Konzelmann et al. 1997). The same time period at Bonsai (2,083 m a.s.l.) yielded similar results as the valley meadow, Q_e comprised 82 % of the energy budget with an average ß of 0.1. Q_e and ß at Bonsai were more comparable to the valley because of similarities in the vegetation community (meadow) compared to the plateau (dwarfed shrubs). The maximum ß aligned with other studies that had highest ß in early spring during snowmelt before the beginning of net carbon storage (Knowles et al. 2015).

The greatest Q* occurred during the *Green Up* period (198 W/m^2), indicating that fluxes that rely on available energy, like ET, may be highest during this time. Although the maximum available energy occurred at *Green Up*, the percent contribution of Q_e to the energy budget remained constant from *Snow Melt* to the end of the *Green Up* (62 – 66 %), increased in the *Peak Growing Season* (86 %), and surpassed Q* during *Senescence*. Reduced available energy, due to shade, provided seasonal available energy values comparable to those experienced in the closed alpine aspen forest understory at 2,049 m a.s.l. (Flerchinger et al. 2010). They found that the alpine understory had an oasis effect, where water table draw down caused understory vegetation to senesce before aspen trees that continued to transpire because they had access to deeper water

reserves (Flerchinger et al. 2010). Our study found that increasing Q_e at the end of the season may be a result of advection from the surrounding forest that increased Q_e until it exceeded Q^*. This indicates that wetland vegetation entered senescence earlier (due to colder temperatures, overnight frost, and decreased soil moisture), while trees in the surrounding forest continued to transpire.

2.5.2 Temporal and Spatial Patterns of Shade

Shade had a strong influence on components of the energy budget throughout the study as it changed in intensity and spatial distribution from *Snow Melt* to *Senescence*. Temporally, June and July received less shade than August and early September, which influenced seasonal growth stages. This was evident as hours of shade per day decreased from *Snow Melt* (2.3 hrs/day) into *Green-Up* (2.1 hrs/day), then increased into *Peak Growing Season* (2.8 hrs/day) and peaked during *Senescence* (4.9 hrs/day). Spatially, the Southern and Western regions of the wetland received more shade than the North and East (Table 2-3). In June and early July, most of the wetland was shaded for 1 - 2 hrs/day, while only the SW corner was shaded for over 2 hours per day. By the middle of July, more intense shading (>2 hrs/day) covered half of the wetland; and by early August the entire site experienced over 2 hours of shade. The period of *Dynamic Shade* is important to consider when evaluating the energy fluxes at the site, because this is when the wetland surface was fully snow free and vegetation the most productive.

The spatial patterns in shade were similar to results found in other studies of solar radiation distribution and variability in mountain terrain with North-South orientation (Oliphant et al. 2003; Marsh et al. 2012). Across the Tekapo watershed (South Island, New Zealand), Oliphant et al. (2003) found that shade was most prominent in the early morning and late afternoon and was most extensive on the Southern boundaries of steeper and higher elevations. Our study indicates that shade was also greatest in the early morning and late afternoon with its largest influence in the SW corner. The S and W areas had a seasonal average of 3.0 and 2.8 hours of shade per day, compared to 2.1 and 2.5 hours of shade per day in the N and E. This concludes that the average amount of daily intercepted solar radiation was 0.9 , 0.7, and 0.4 MJ greater in the S, W, and E than in the N, respectively. Therefore, over the 96-day study period, the S, W, and E portions of the wetland received 86.4, 67.2, and 38.4 MJ less solar radiation due to the cumulative impact of horizon shade, respectively. These spatial patterns explain the thick snowpack along the western and southern margins of the wetland and why snow remained longer into *Peak Growing Season*, as late as

August in 2018. This has occurred in other years at the site, as seen in Figure 2-9 where the western boundary was snow covered until August 6th (2012). Therefore, over the entire study period, one additional hour of shade per day in the SW corner reduced K↓ by an average of 51 W/m^2 per day, enough to maintain snow later in the season on an annual basis.

2.5.3 Impact of Horizon Shade on Solar Radiation and the Energy Budget

During the period of *Stable Shade,* shade did not influence K↓ because it mostly impacted the wetland in morning and evening hours when K↓ was low (Figure 2-11). However, when shade increased during *Dynamic Shade*, radiation was not only intercepted in the morning and evening but also during the high radiative input of mid-day hours, significantly reducing total daily K↓ (Figure 2-11). On average, each hourly increase in shade during *Dynamic Shade* reduced actual K↓ by 13 % (32 W/m^2) and modeled K↓ by 10 % (35 W/m^2) (Figure 2-12). The difference between modeled and actual K↓ was because the model only accounted for perfect clear sky conditions while actual observations were the best available days but may still have had some interference from clouds, fog, and/or forest fire smoke. The study by Oliphant et al. (2003) found that shade reduced modeled K↓ an average of 45.2 W/m^2 (18 % per day) across the whole watershed, and that higher elevations (1,489 m a.s.l.) received 11 % less K↓ than lower elevations (707 m a.s.l.). Our study performed a more detailed analysis than Oliphant et al. (2003) because their work only accounted for one day (February 12th; peak growing season in the southern hemisphere), compared rasters as shaded vs. non-shaded in a daily interval (i.e. no hourly ranges), and examined an entire watershed (where over 70 % of total surface area was <1,300 m a.s.l.). Therefore, Oliphant et al (2003) provided a more general analysis for K↓ at a large basin-wide scale, while our study performed a more detailed characterisation of shade but within a smaller confined subalpine wetland. Since modeled K↓ found close agreement with Oliphant et al. (2003) around the two-hour margin, it can be assumed that 2 hours of horizon shade per day reduces K↓ by an average of approximately 19 % on clear sky days at ecosystems with North-South orientation in complex terrain.

Results from this study found that each hourly increase of shade at Bonsai reduced K↓ and Q* by 13 % and 16 %, respectively. Oliphant et al. (2003) also found decreases in Q* with elevation and surface complexity, but by small daily margins (20 %). The literature has found that radiation-use efficiency, or the amount of biomass accumulated per intercepted K↓, across a

variety of ecosystems was higher for diffuse radiation than direct radiation (Gu et al. 2002; Urban et al. 2007).   Therefore, when shade decreased K↓ throughout *Peak Growing Season*, diffuse radiation helped maintain ET, which stabilized Qe, and supported plant productivity.

2.5.4 Implications on Alpine Hydrology and Next Steps

Results from this study found that horizon shade reduced solar radiation input during critical times throughout spring snowmelt and created favourable conditions to maintain snow later into the season, despite potential increases in overall air temperatures. This was most evident along the southern and western boundaries of the wetland (that received the greatest amount of shade). Therefore, shade was an important mechanism for snowpack sustenance, which helped maintain patches of thick snow and contribute late summer runoff in the late season when water supplies are low.

Although this study examined the influence of shade on the energy availability of a subalpine wetland, there remain knowledge gaps that still need to be addressed. To close the water balance and help advance the development of hydrological models for complex mountainous terrain, further studies are required to understand the relationship between evaporative fluxes and horizon shadow, and other shadow types.   It is known that snowmelt into late summer is an important water source in the Rocky Mountains because it contributes summer runoff to drier regions downstream (Fang et al. 2013).   However, warmer temperatures and a shift in climate trends have altered the timing and characteristics of these historically stable snow packs (Parker et al. 2008). Currently, there are more winter days with air temperatures above 0 °C than in the past (Lapp et al. 2005), which has decreased spring snow cover (Brown & Robinson, 2011), and resulted in a thinner snowpack with earlier runoff and lower streamflow (Stewart et al. 2004; St. Jacques et al. 2010). Therefore, ET and snow water equivalence (SWE) must be quantified within shaded subalpine wetlands to help determine how water is used within these systems, and their importance to downstream water contributions.

2.6 Conclusions

The energy budget of a sub-alpine wetland in the Canadian Rocky Mountains was analyzed throughout the growing season from June to September. The temporal patterns and daily ranges of energy fluxes, measured at our study site, were consistent with those reported for similar sites

in the literature. Incoming solar radiation and components of the energy budget were highest early in the season, during *Snow Melt* and *Green-Up* periods, and decreased later into the season. Most of our wetland remained snow covered during the time of annual maximum solar radiation input and this snowpack persisted longer into the growing season, due to increased horizon shade. Shade reduced the magnitude of all components of the energy budget and may prove to be an important mechanism for moisture control during *Peak Growing Season* by reducing evaporative losses. However, the results from this study only represent one ecosystem within the larger mosaic of wetlands, meadows and tundra found in mountain regions. Since decreases in available energy differ based on localised topography, additional studies are required to enhance the knowledge of energy budget dynamics of shaded ecosystems across a variety of mountain networks. Once such studies become available, we will be able to more accurately quantify the role of shade on the energy budget within complex terrain and its contribution to Late Season runoff downstream.

Chapter 3:   Manuscript 2: Analysis of growing season carbon and water fluxes of a subalpine wetland in the Canadian Rocky Mountains: implications of shade on ecosystem water use efficiency.

3.1 Introduction

Alpine regions are an important regulator in the global water balance. Although mountainous terrain only covers 20 % of the Earth's land mass, they contribute 40 to 60 % of annual surface flow (Ives & Messerli, 1999; Grusson et al. 2015). As a result, many of the world's major river networks originate from alpine sourced headwater basins, where downstream runoff from snowmelt may entirely comprise regional stream flow (Viviroli et al. 2011). In areas that receive low summer precipitation, such as the semi-arid Western United States and Canada, alpine headwaters provide a natural and continuous water source for irrigation and municipal water supplies to over 60 million people (Barnett et al. 2005; Bales et al. 2006). Because of their large hydrological contributions, literature often refers to mountains as the "Water Towers of the World" (European Environment Agency, 2009; Immerzeel, 2008). The Rocky Mountains represent Western Canada's Water Tower, since they store and distribute large quantities of water resources across the western prairie provinces and north-central states. The Rockies are the primary water source for over 13 million people that live in cities and rural communities across British Columbia, Alberta, Saskatchewan, Manitoba, Washington, and Oregon (Fang et al. 2013). Runoff from the Rockies also supplies the Saskatchewan, Athabasca, Columbia, and Fraser Rivers - important headwater resources for agriculture and industry operations downstream (Fang et al. 2013). The South Saskatchewan River Watershed is one such example, where municipal water supply and industry are heavily reliant on runoff from the Rocky Mountains (Figure 1-1).

Alpine wetlands provide many ecosystem services to mountain landscapes and nearby lowlands. They are widespread across alpine regions, but favour the physical and environmental conditions present within intermountain basins and upper mountain valleys (Windell et al. 1986). They provide many important hydrological and ecological functions, such as flood mitigation, water for consumption and irrigation, and support for important ecological habitats (Aber et al. 2012). Wetlands are also an important ecosystem in regulating the global climate and are large contributors to carbon (C) storage. Broadly speaking, all wetlands store 12 to 15 % of the global

33

C pool (Cao et al. 2017), of which alpine wetlands contribute 2.5 % in storage (Zhao et al. 2010). In the Western U.S.A. alone, 70 % of the carbon sink is located above 750 m.a.s.l, in landscapes covered by 85 % hills and mountains (Schimel et al. 2002; Desai et al. 2011). As a result, alpine regions are extremely diverse and contain hotspots of high soil organic carbon (SOG) in moist to wet meadows, moderate SOG in dry meadows, and low SOG in fellfield (i.e. alpine tundra) (Knowles et al. 2015).

Water use efficiency (WUE) is a useful metric to analyse the interaction of water and C fluxes of an ecosystem, as it is a proxy that quantifies the carbon-uptake (GPP), through photosynthetic process, per gram of water used through evapotranspiration (ET) (Rosenberg et al. 1983). It has been measured on numerous scales including: ecosystem, plant, and leaf level and is often used in agricultural and crop science (Medrano et al. 2015). Recently, WUE has also been used in studies of alpine wetland ecosystems to help evaluate seasonal water resources (Hu et al. 2008; Han et al. 2013; Strobl et al. 2017; Quan et al. 2018). Studies have shown that WUE often decreases with increased water availability, resulting in lower WUE at high elevations that experience greater water supplies (Han et al. 2013). Other studies have identified that ecosystem WUE adapts to environmental conditions, like the microclimate and available energy over the course of a day (Strobl et al. 2017). Therefore, WUE can be a useful metric to help evaluate the influence of various microclimatic changes in alpine environments on C and water.

The goal of this manuscript is to explore the effect of complex terrain on water and carbon fluxes at a sub-alpine wetland influenced by horizon shade. The first manuscript of this thesis (Chapter 2) identified the negative impacts of seasonal shade on available energy budgets at the site over the course of the growing season. This manuscript will: 1) quantify the seasonal patterns of carbon and water exchange at the wetland; and 2) investigate if and how they are impacted by seasonal shading. Given that water fluxes are related to available energy through the latent heat of evaporation, we hypothesize that ET will be negatively affected by horizon shade and potentially cause an increase in WUE (if C-fluxes are unaffected) or constant WUE (if C-fluxes also decrease).

3.2 Study Site

The study was conducted at Fortress Mountain (50.82 °N, 115.21 °W), a non-active alpine ski resort, located in the Kananaskis Range of the Canadian Rocky Mountains. Fortress Mountain is located 30 km South of the town of Canmore and 80 km West of Calgary, Alberta (Figure 3-1 subsets: A, B). The topographic boundary of the site is outlined by a headwall (~500 m) to the south, an ephemeral tarn on the North, and ridges (~150 m) to the East and West (Figure 3-1, subset: C). The alpine wetland study site referred to as Bonsai, is 1 ha in size (Figure 3-1), and is classified as a freshwater marsh/wet meadow using methods of Windell et al. (1986). Bonsai is mostly flat with a moderate increasing slope of 6 degrees (2083 to 2086 m) from the tarn to the base of the talus slopes (50 m). Because of the headwall to the South and ridge to the East, the wetland is shaded for long durations of time across the day and season, which promotes a thick snowpack, long snow-covered period, an extended spring melt period, and a constrained growing season (Figure 3-2).
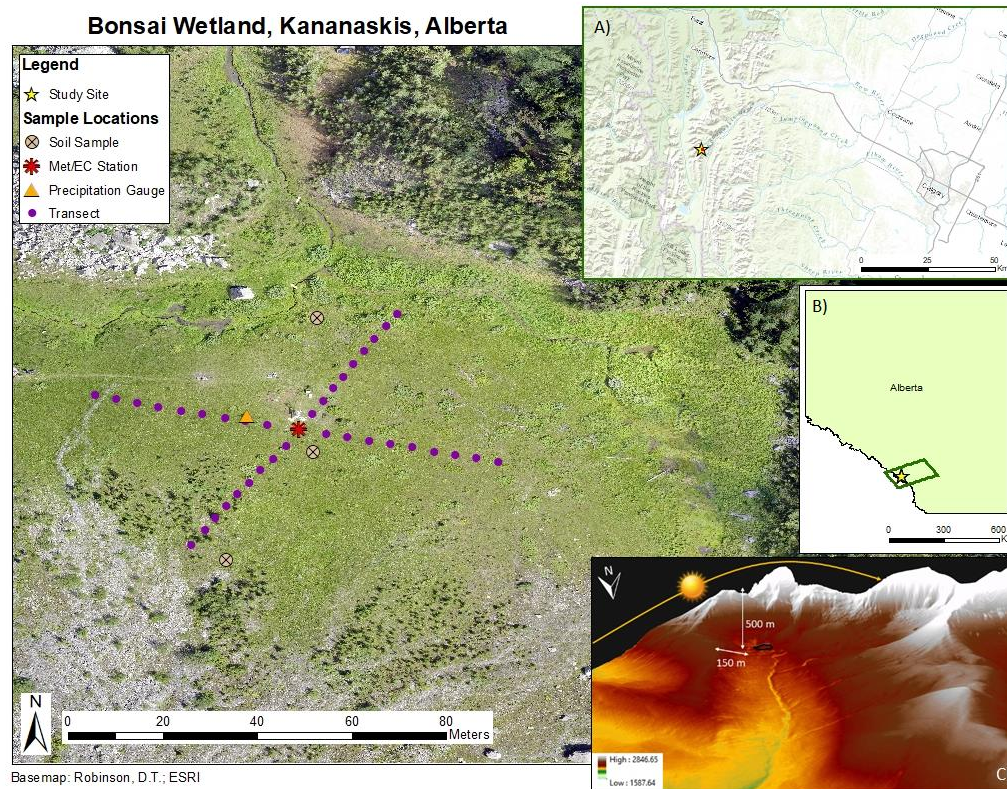
Figure 3-1: Site map Bonsai wetland, showing the location of equipment/sampling, its location in the province of Alberta and the Eastern Rockies (A/B), and LIDAR imagery of the basin with daily sun path and topographic boundary elevations (C).

Surface water from two streams meet at a confluence in the North-Central section of the wetland which drains into the tarn, then Galatea Creek and downslope to the Kananaskis River (a tributary to the Bow River). The two main stream branches follow the Eastern and Western margins of the wetland and are sourced from springs that emerge at the base of the talus deposits (Christensen, 2017). During spring melt, the Eastern stream floods and water pools above the surface in a confined area of the North-East corner for several weeks. Throughout the growing season, the Western stream continues to flow, but the Eastern stream dries by midseason.

Figure 3-2: Images of the seasonal evolution of Bonsai during A) *Snow Cover***, B)** *Snow Melt***, C)** *Green Up***, and D)** *Peak Growing Season***. Images were taken during the 2018 field campaign on A) June 8th, B) June 18th, C) July 6th, D) July 26th.**

Climate conditions within the Kananaskis Valley are indicative of continental air masses with long and cold winters and an average air temperature of -15 °C from January to March (DeBeer & Pomeroy, 2009). Average annual precipitation is 900 mm in the valley and sub-alpine but increases to well above 1140 mm in elevations greater than the treeline (Storr, 1967). Snow cover remains from November to June, because of cold temperatures and a large contribution of precipitation as snowfall (65 – 70 %) (DeBeer & Pomeroy, 2009; Marsh et al. 2012). The melt period often begins in April, as temperatures increase, and finishes in July with maximum solar radiation and temperature (DeBeer & Pomeroy, 2009). A nearby Environment and Climate Change Canada (ECCC) monitoring station (ID 3053600: 51.03 N, 115.03 W) identifies the 30-year (1981 – 2010) average monthly temperature of June, July, August, and September as 11.4 °C,

14.5 °C, 13.8 °C, and 9.4 °C, respectively, with an annual minimum of -6.2 °C in December and maximum of 14.5 °C in July (Figure 2-4). Average annual precipitation is 639.3 mm, with 119.4 mm, 64.9 mm, and 70.8 mm falling over the months of June, July and August.

There were noticeable spatial differences in the soil (Table 3-1) and vegetation (Figure 3-3) characteristics across the wetland. There was a thin layer of pervious well-sorted sand above a semi-pervious layer of very fine silt in the North (0-10 m in Figure 3-3, Table 3-1) and Middle portions of the wetland (20-30 m in Figure 3-3, Table 3-1). The Middle section of the meadow (20-30 m) had the highest percent of organic material (LOI) and was defined by silt and clay that was moist and plastic, but not fully saturated (Christensen, 2017). Across the wetland, soil surpassed its moisture threshold at 2m and increased in saturation with depth (Christensen, 2017). In terms of vegetation cover, the Northern section of the wetland was dominated by *Erigeron caespitosus*, of the family *Asteraceae,* native to the Rocky Mountains Region in Western Canada (Figure 3-3). The Middle section was dominated by shade tolerant species like *Equisetum*, *Salix, Castilleja raupii,* & Litter (Figure 3-3). Litter was greatest across the Middle of the wetland, because there was a high presence of S*alix,* a broadleaf shrub that sheds its leaves. Further South and closest to the headwall, groundcover vegetation was largely brown moss (Figure 3-3).

Table 3-1: Soil characteristics from North to South (N➔S) along an increasing elevational gradient, and exposure to shade.

	North		Middle		South
	Stream Confluence (0-15.5cm)	**Stream Confluence (15.5-31cm)**	**Tower (0-9.5cm)**	**Tower (9.5-29.5cm)**	**Headwall (0-15cm)**
Avg Ksat (cm/s)	$1*10^{-1}$	$5*10^{-5}$	$7*10^{-2}$	$9*10^{-5}$	$1*10^{-1}$
Avg Ksat (m/day)	95.00	0.04	59.16	0.08	107.61
BD (g/cm³)	1.64	1.50	1.10	1.12	0.49
LOI (%)	5.22	4.91	10.20	6.80	6.92
Permeability	Pervious	Semi-pervious	Semi-pervious	Semi-pervious	Pervious
Texture	Silt Loam	Silt Loam	Loamy Sand	Sandy Loam	Loamy Sand

Figure 3-3: Groundcover and vegetation survey results along 3 transects from the stream confluence to headwall (N→S).

3.3 Materials and Methods

3.3.1 Meteorological Data

A meteorological tower was installed at Bonsai in the centre of the wetland and instrumented with meteorological equipment to monitor the environmental conditions from June 7th to September 10th, 2018. Measurements were taken every 10 seconds and averaged to half-hourly values that were recorded on a 9210XLite data Logger (Sutron, Stirling, Virginia, USA). Power to the station was provided by a 12-volt deep cycle battery that was charged by a 40-watt solar panel, equipped with a SunSaver-20L solar controller. Wind speed was measured by an R.M. Young 05103 – 10A anemometer (Traverse City, Michigan, USA) at a height of 3.8 m. Net radiation was measured with by a net radiometer (NR Lite, Kipp and Zonen, Delft, Netherlands) and photosynthetic active radiation was measured by a quantum sensor (Li-Cor 2319, LI-COR, inc., Lincoln, Nebraska, USA) at 3.05 m. Air temperature (T_a) and relative humidity (RH) were measured with a Vaisala

HMP-155 probe at 3.4 m (Vaisala, Helsinki, Finland). Two soil heat flux plates (Husk Flux Thermal Sensor HFP01, Delft, Netherlands) were placed under the soil surface at 5 cm depths to measure average ground heat flux. Two ECH2O EC-5 sensors (Meter Group, Hopkins, Washington, USA) measured the average soil moisture at a 10 cm depth below the surface, and soil temperatures (T_s) was measured at 3 depths (2 cm, 5 cm, & 10 cm) with Li-Cor 7900-180 soil temperature probes (LICOR Inc., Lincoln, Nebraska, USA). Precipitation was measured by a tipping bucket rain gauge (Onset HOBO, Hoskin Scientific, Burnaby, British Columbia, Canada) in a forested clearing 350 m North of the study site, but at a similar elevation. Additionally, to capture spatial variability in soil temperature and moisture conditions, two transects were set up along the N-S and W-E cardinal directions across the wetland. Manual weekly soil moisture measurements were taken in 3 m intervals, using the Hydrosense 2 (Campbell Scientific, Logan, Utah, USA) at a depth of 20 cm.

3.3.2 Eddy Covariance Measurements

Water, carbon and momentum fluxes were measured at the site with an Eddy Covariance (EC) system deployed at the meteorological tower from June 7th to September 10th. The EC system consisted of a 3D sonic anemometer (CSAT3; Campbell Scientific Inc., Logan, Utah, USA) and an open-path infrared CO_2 / H_2O gas analyzer (IRGA) (LI-7500, LI-COR Inc., Lincoln, Nebraska, USA) mounted 3 m above the surface onto the meteorological tower. Fluxes were sampled at a frequency of 10 Hz and averaged over half an hour, with half-hourly averages recorded on a CR1000 datalogger (Campbell Scientific, Logan, Utah, USA). Detailed methods for EC processing are listed in the first manuscript, in addition to, Appendix 1.

3.3.3 Hill shade Model

Bonsai tower coordinates were input into www.suncalc.org (Hoffmann, 2018), a free publicly available website that delivers solar data for any date and time across the globe. Suncalc provided the azimuth, altitude, and shadow length in 15-minute intervals for clear sky days across the study period (June 7th – September 10th). Clear sky days were selected based on daily field observations and through near perfect daily K↓ bell-curve plots. The records for clear sky days (n=31) were downloaded and compiled into a single table. Negative altitude values, or time that the sun was below the horizon, were removed to avoid any error in the hill shade calculation. This data was

then loaded into ArcMap (v10.6) alongside a Digital Elevation Model (DEM) for the region to run the hill shade analysis. First, hill-shade rasters were created with the hill shade tool and were then clipped to the study area. Each hill-shade raster was reclassified to associate shadows with a value of 0 and everything else with a value of 1. The raster calculator was used to create one hill-shade raster that represented the sum of all the rasters for each day. Each cell value for the summed hill-shade raster was converted to total hours shaded, for each clear sky day, with 11 equal interval classes from 1 to 11 hours, using the following equation,

$$Hours\ shaded = \frac{(Shade\ value) * 15\ minutes}{60\ minutes/hour} \tag{1}$$

where shade value was the cell value from the summed hill-shade raster.

3.3.4 Statistical Analysis and Calculations

All statistical analyses were performed and summarized with packages dplyr, reshape2, tidyr, and forcats then illustrated with ggplot2 in RStudio (RStudio Team, 2016). Prior to any analysis, data was assessed for normality through a Shapiro-Wilks normality test. Results from the Shapiro-Wilks test concluded that all daily data used within this analysis was normaly distributed ($p > 0.05$), other than the hill shade model output. Since the hill shade results are the independent variable and the remainder of the data was accepted by the Shapiro-Wilks test, parametric testing was acceptable to use in the statistical analysis.

Hill shade results from manuscript 1 (Chapter 2) was used in the statistical analysis to help understand the influence of shade on the water and carbon fluxes at the site. A linear regression model was used to understand the influence of shade (independent variable) on the water and carbon fluxes (dependent variables). Since the ouput from the hill shade model was the independent variable, parametric testing was acceptable to use in this section of the study. To help isolate shade in the statistical analysis, the data was divided based on *Stable Shade* with consistent average daily shade (June 7th to July 30th) and *Dynamic Shade* with increasing average daily shade (July 31st to September 10th).

Meteorological data was used in the calculation of potential evapotranspiration (PET), used in analysis and discussion in this study. PET was calculated using the Priestley-Taylor equation (Priestley & Taylor, 1972),

$$PET = \alpha \frac{s}{s+\gamma} (Q^* - Q_G) \qquad (2)$$

where, α is a model coefficient (1.26), s is the slope of the saturation vapour density curve (g/m^3), γ is the psychrometric constant (66 Pa K^{-1}), Q* is net radiation (W/m^2), and Q$_G$ the soil heat flux (W/m^2).

3.4 Results

3.4.1 Climatic Conditions

Bonsai climate was defined by cool air temperature and low precipitation, common in mid-latitude upper continental elevations (DeBeer & Pomeroy, 2009; Marsh et al. 2012). The 2018 study period displayed similar temperature and precipitation trends, as those reported by the Environment and Climate Change Canada (ECCC) climate normals (1981 – 2010) for the region. Average air temperature during the study was 9 °C (±4.1), with a daily maximum of 18.6 °C on August 10th and a daily minimum of 0.8 °C on June 11th (Figure 3-4). The soil surface remained frozen until June 20th and then rapidly increased in temperature from -0.3 °C to 7.4 °C over a three-day period (Figure 3-4). The spring thaw aligned with when snow free areas began to form around the tower (Figure 3-2B). Average monthly air temperatures during the 2018 study period fell within 2 standard deviations (except for September) of the ECCC 30-year climate normals for the region (Figure 2-4). Rainfall from June to August reached 339 mm at Bonsai, similar to the historic seasonal average across Marmot Creek Research Basin (342 mm), located 14 km North in the Kananaskis Range (DeBeer & Pomeroy, 2009).

Data was analyzed focussing on four key time periods, which we refer to as "seasonal phases" that were defined by snowpack thickness and vegetation phenology observed throughout the study (Figure 3-2). The seasonal phases were: *Snow Melt* (June 7th to 23rd); *Green-Up* (June 24th to July 20th); *Peak Growing Season* (July 21st to August 23rd); and *Senescence* (August 24th to September 10th). The beginning of the study period had frequent and intense precipitation events, where two individual days received upwards of 33 mm (Figure 3-4C). Snowfall was captured on a time lapse camera as late as July 2nd and began again in the Fall on August 29th. In total June, July, August, and September (2018) received 49 mm of cumulative precipitation less than the 30-

year climate normal, where only July and September received the average amount of precipitation. Therefore, 2018 had typical temperatures with less precipitation than normal.
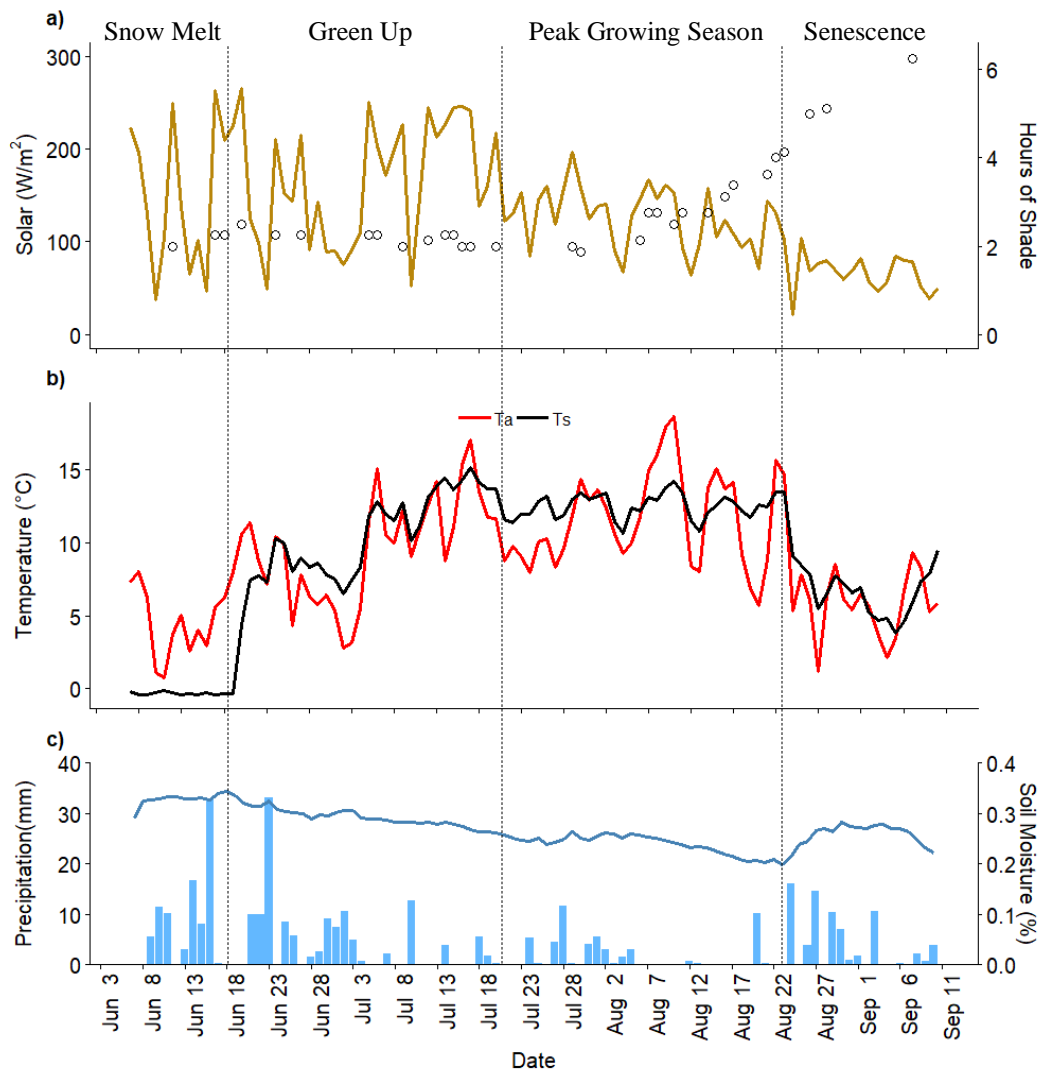
Figure 3-4: Trends in weather data over the 2018 field season: a) incoming solar radiation (W/m²) and hours of shade per day, b) air temperature (Ta) and surface soil temperature (Ts) at 2cm, and c) precipitation defined by rain (plotted as bars), and soil moisture (plotted as the line).

The highest mean daily volumetric moisture content (VMC), 34.3 %, was measured in the middle of the wetland (20-30 m from the stream) at our meteorological station, on June 18th, and the lowest VMC of 20.0 % was observed on August 23rd at the same location. However, VMC also varied spatially, as was shown by our weekly manual VMC measurements (Figure 3-5). The manual measurements showed that in July, VMC was higher near the stream and lower in the middle of the wetland, while in August the middle of the wetland was more saturated than the

stream banks. This was likely a by-product of well sorted soil near the stream (Table 3-1) that limited the ability for moisture retention once the streams ran dry, and greater litter cover in the middle (Figure 3-3) that helped keep soils moist. South of the tower, with increased proximity to the headwall, there was a rapid decline in VMC because of coarser textured soil, gravel, and debris from the headwall and talus slopes.
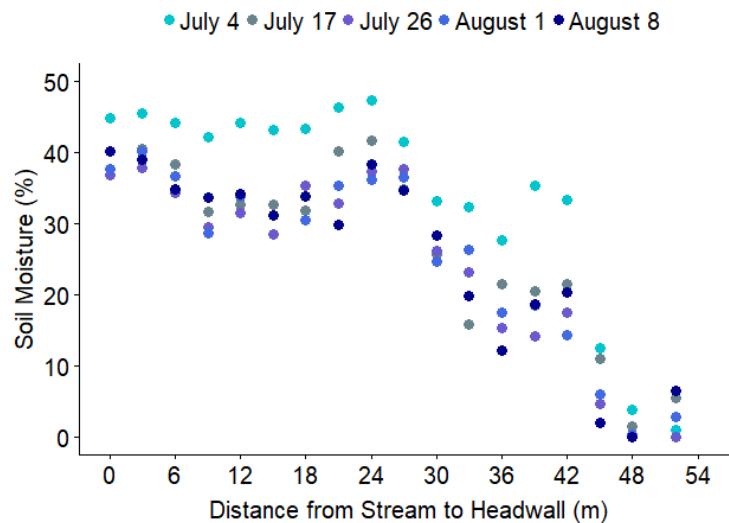
Figure 3-5: Spatial and temporal trend in soil moisture from the stream confluence (0 m) to the headwall (54 m).

3.4.2 Subalpine Wetland Evapotranspiration

Across the entire 2018 study period, cumulative evapotranspiration (ET) and potential evapotranspiration (PET) reached 158 mm and 176 mm at the site, respectively (Figure 3-6). During S*now Melt* both ET (0.8 to 2.7 mm/day) and PET (1.1 to 3.3 mm/day) increased because of evaporation from snowmelt runoff. ET and PET continued to increase into G*reen Up* when they reached their daily maximum from July 12th to July 17th, due to large inputs from snowmelt evaporation and transpiration from wetland vegetation, including trees and shrubs (ET 3.5 mm/day, total of 21 mm; PET 4.5 mm/day, total of 27 mm, respectively) (Figure 3-6). In total, *Green Up* contributed 57.5 mm of the seasonal cumulative ET, equivalent to 36.5 % of all ET in only 25 % of the study period. Daily ET contributions were largest during G*reen Up* because incoming solar (K↓) and net radiation (Q*) remained high following the solar maximum and provided large energy contributions to sustain latent (Q_e) and sensible (Q_h) heat fluxes, as shown

in Chapter 2. After *Green Up,* ET was influenced by the increasing horizon shadow effect and followed a decreasing trend similar to K↓ through the remainder of *Peak Growing Season* and into *Senescence* (Figure 3-6; Figure 3-4). Therefore, *Peak Growing Season* ET and PET were lower than *Green Up* with daily averages of 2.0 and 2.2 mm/day and cumulative totals of 66.6 and 74.2 mm, respectively. This represented a larger contribution than *Green Up* with 42.2 % of total ET, but over a longer period of time (37 % of study period). During *Senescence,* ET remained low (0.94 mm/day; total of 17 mm) and contributed only 10.8 % to total ET. Therefore, the *Green Up* and *Peak Growing Season* provided the largest contribution to seasonal ET (124.1 mm, 78.7 % of cumulative ET) during the course of this study, driven by higher K↓.
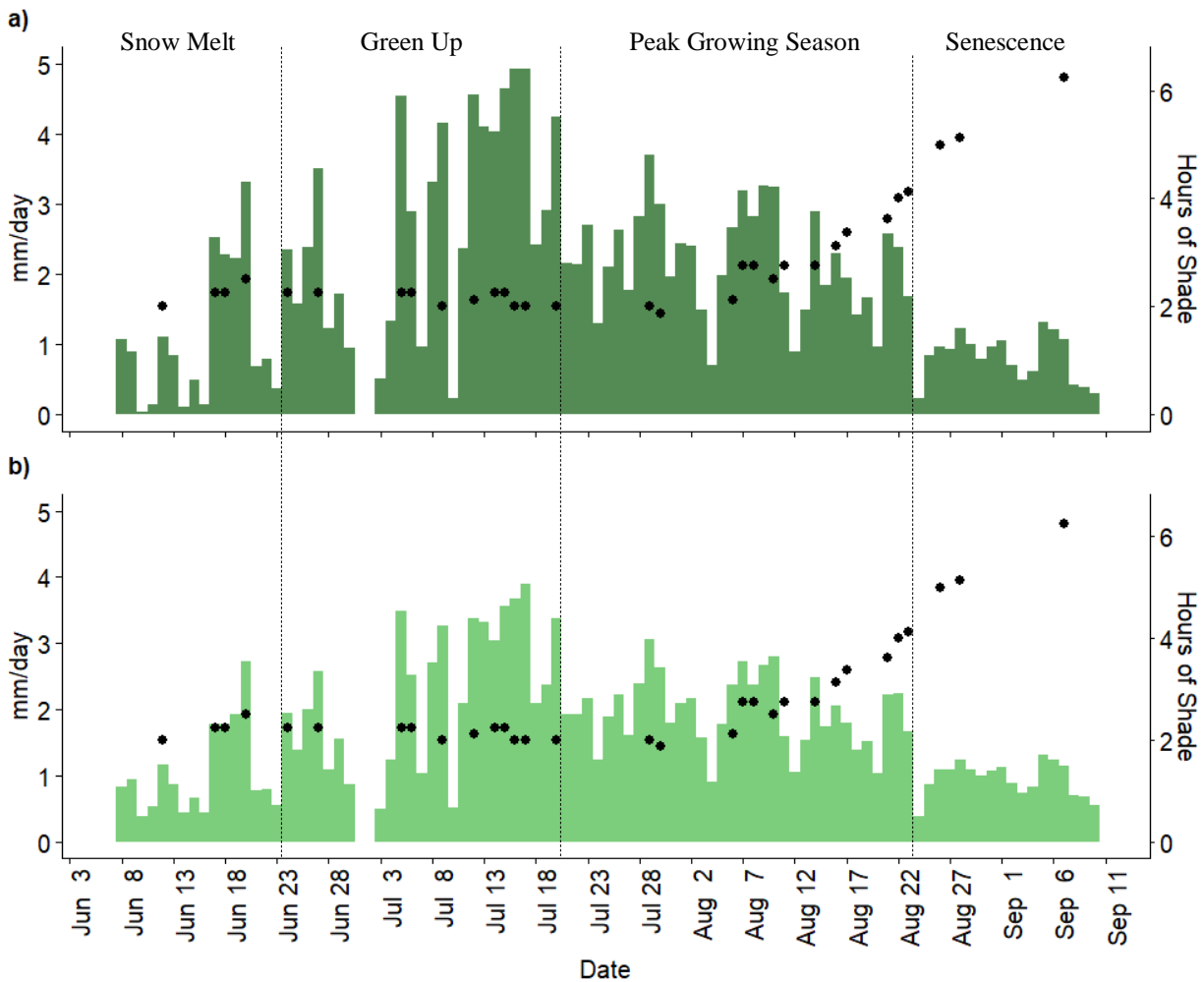
Figure 3-6: Daily average (a) Potential Evapotranspiration (PET), and (b) Actual Evapotranspiration (ET) plotted alongside the average hours of shade per day (black dots) at Bonsai Wetland, Fortress Mountain, Alberta, 2018.

3.4.3 Subalpine Wetland Carbon Flux

The carbon flux was extremely variable during *Snow Melt* and represented a strong source (defined as Net Ecosystem Exchange: NEE, source indicated by positive value), releasing an average of 1.4 g C m^{-2} day for a total release of 24 g C into the atmosphere (defined as Ecosystem Respiration: R$_{eco}$) over this period (Figure 3-7). The wetland then fluctuated between a source and sink during *Green Up,* where variability in C uptake/release continued until July 6th as the ground surface became increasingly snow free. Following July 6th, Bonsai was a C sink (Negative NEE) until *Senescence*. C sink strength increased throughout *Green Up,* when the wetland took up an average of 0.58 g C m^{-2} day for a total carbon sink of 16 g C / Green Up season. Maximum productivity (defined as Gross Primary Production: GPP) occurred once the entire site became snow free and green (July 29th to August 2nd) with an average daily GPP, R$_{eco}$, and NEE of 6.4, 4.5, and 1.8 g C m^{-2} day, respectively. C sequestration largely took place between the hours of 08:00 and 19:00 during *Peak Growing Season* from the middle of July to the end of August (Figure 3-10). At this time, cumulative C uptake was high enough to offset C emissions from the *Snow Melt* period and shift Bonsai into a cumulative sink (Figure 3-7b). Ecosystem sink strength continued to increase between July 29th to August 2nd , with an average daily C uptake of 6.4 g C and an average C release of 4.5 g C for a NEE of 1.78 g C. Following the seasonal maximum on July 30th, there was a decreasing trend in the C flux for the remainder of the study. During the *Senescence* period, the site remained a consistent C sink with a net C uptake of 0.42 g C m^{-2} day; except for September 7th which had a NEE of 3.3 g C. NEE spiked on September 7th because of an abnormally warm day (9.4 °C) during *Senescence* when the average daily air temperature was only 5.5 °C. Over the entire study period, Bonsai was a net sink of 63 g C; however, it may be possible that Bonsai is a net annual source because of high C emissions found during *Snow Melt* when the surface was snow covered.
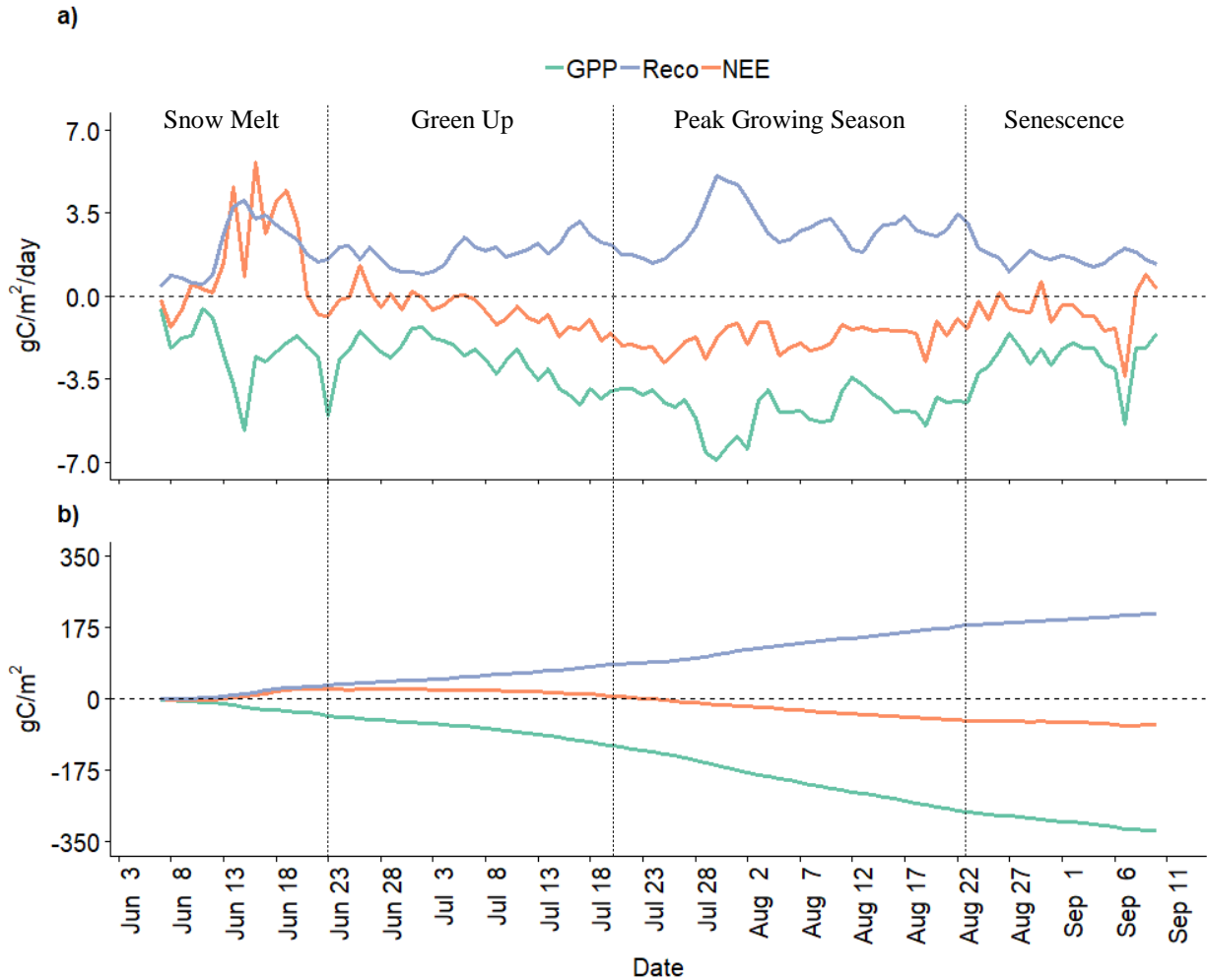
Figure 3-7: Average (a) Daily carbon fluxes (g C m^{-2} day), and (b) Cumulative carbon fluxes (g C m^{-2} day). Carbon fluxes defined as Ecosystem Respiration (R_{eco}), Net Ecosystem Exchange (NEE), and Gross Primary Production (GPP), Bonsai Wetland, Fortress Mountain, Alberta, 2018.

3.4.4 Subalpine Wetland Water Use Efficiency

From *Green Up* to *Senescence*, Bonsai had an average WUE of 2.9 g C (kg H$_2$O)$^{-1}$ day ($\pm$ 0.80) and was highest during periods of peak productivity (*Growing Stage*) and lowest during shoulder seasons (*Green Up & Senescence*) (Table 3-2). Maximum WUE (5.3 g C (kg H$_2$O)$^{-1}$) occurred on August 20th and minimum WUE (1.4 g C (kg H$_2$O)$^{-1}$) occurred on June 29th. During the seasonal maximum on August 20th, vegetation was highly productive, but was water stressed; while on the seasonal minimum (June 29th) vegetation was not yet productive but had a large water store. Periods surrounding the maximum and minimum illustrate the seasonal trends in WUE; during

46

Green Up and *Senescence* Bonsai had low daily averages (2.4 and 2.9 g C $(kg\ H_2O)^{-1}$, respectively), while in *Peak Growing Season* there was high daily averages (3.35 g C $(kg\ H_2O)^{-1}$).

Table 3-2: Average daytime ($Q^* > 10\ W/m^2$) Water and carbon fluxes over the study period on clear sky days: Snow Melt (June 7-23), Green Up (June 24 to July 20), Peak Growing Season (July 21 to August 23), and Senescence (August 24 to September 7). Standard deviations (S.D) are listed below in parentheses.

	ET (mm)	GPP (g C)	Reco (g C)	NEE (g C)	WUE g C $(kg\ H_2O)^{-1}$
Snow Melt	1.80	-1.81	1.89	0.20	2.30
(June 7th – June 23rd)	(± 0.6)	(± 0.8)	(± 0.9)	(± 0.3)	(± 0.7)
Green Up	3.05	-2.90	1.70	-1.18	1.90
(June 24th – July 20th)	(± 0.6)	(± 0.9)	(± 0.3)	(± 0.8)	(± 0.4)
Peak Growing Season	2.14	-4.61	2.20	-2.39	3.39
July 21st – Aug 23rd	(± 0.5)	(± 0.8)	(± 0.6)	(± 0.5)	(± 0.4)
Senescence	0.98	-2.19	1.07	-0.97	3.41
(Aug 24th – Sept 10th)	(± 0.1)	(± 0.1)	(± 0.2)	(± 0.3)	(± 0.9)
Average	2.31	-3.41	1.87	-1.49	2.72
	(± 0.8)	(± 1.3)	(± 0.6)	(± 1.1)	(± 0.9)

Statistical analysis found that WUE was negatively correlated with ET, but positively correlated with GPP over the entire study period, confirming that increased ET during *Green Up* led to a lower WUE and a greater GPP in *Peak Growing Season* resulted in a higher WUE. WUE had a stronger relationship with GPP ($p < 0.001$, $R^2 = 0.32$) than ET ($p < 0.05$, $R^2 = 0.16$), indicating there was a strong influence from a variety of environmental variables over the study period (i.e. VMC, T_a, and T_s, K$\downarrow$ & Shade) (Table 3-3). During *Dynamic Shade* (when shade was rapidly increasing), WUE had a non-significant relationship with shade ($p > 0.05$, $R^2 = 0.08$).

3.4.5 Effects of Shade on subalpine wetland carbon and water fluxes

ET had a statistically significant relationship with shade, where a greater horizon shadow led to lower evaporative losses. Actual ET and PET had statistically significant negative relationships ($R^2 = 0.66$, $p < 0.01$; $R^2 = 0.66$, $p < 0.01$, respectively) with hours of shade per day (hrs/day) during *Dynamic Shade* (Figure 3-8b), but not during *Stable Shade* ($R^2 = 0.04$, $p > 0.05$; $R^2 = 0.02$, $p > 0.05$) (Figure 3-8a). During *Dynamic Shade*, each hour of shade decreased actual ET losses by

0.42 mm/day (y = -0.42 x +3.3) and potential ET losses by 0.57 mm/day (y = -0.57 x +4.3). Therefore, the overestimation of PET was larger early in the season during the period of constant shade (ET:PET = 0.80) than late in the season when shade increased (ET:PET = 0.97). The ET:PET ratios align with conclusions drawn from Chapter 2, that found the energy budget was strongly tied to the hours of shade per day (Figure 2-12). Therefore, there was a statistically significant relationship between ET and available energy over the study period (R^2 = 0.79, $p < 0.01$), indicating that increased shade (and lower available energy) decreased evaporative losses and established a greater potential for water storage.
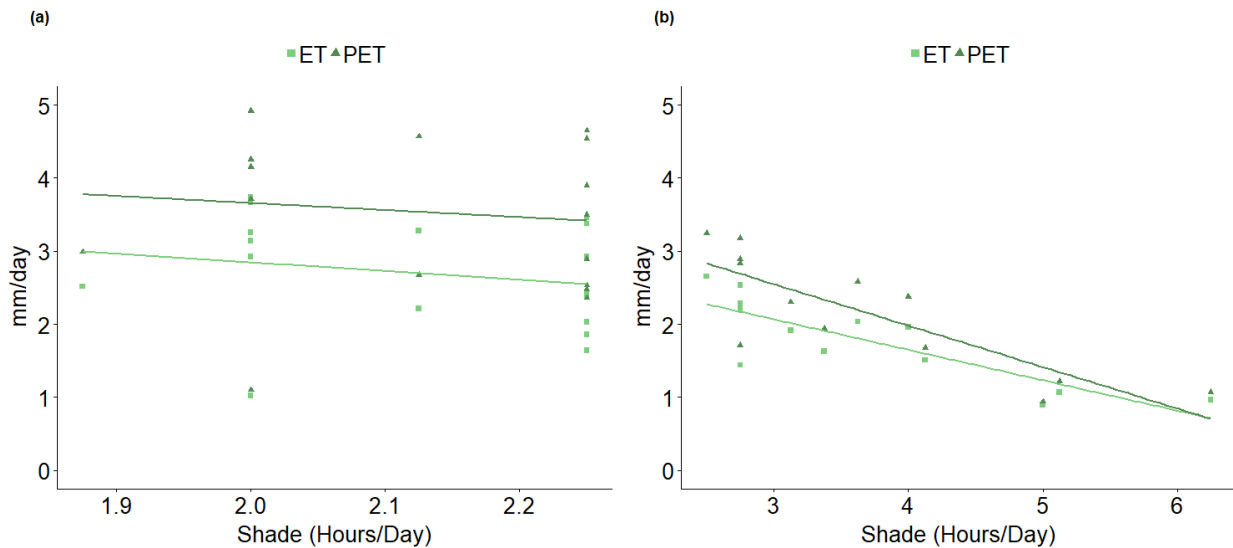
Figure 3-8: Relationship between hours of shade and Actual Evapotranspiration (ET) and Potential Evapotranspiration (PET) on clear sky days during the periods of (a) *Stable Shade*, and (b) *Dynamic Shade* at Bonsai wetland, Fortress Mountain, Alberta, 2018.

Bonsai carbon flux was also influenced by shade and had a statistically significant negative relationship with GPP (R^2 =0.75; $p < 0.01$) and R_{eco} (R^2 = 0.39, $p < 0.05$), and a statistically significant positive relationship with NEE (R^2 = 0.73, $p < 0.01$) during *Dynamic Shade* (Figure 3-9b). This indicates that each hourly increase of shade during *Dynamic Shade* decreased GPP by 0.77 g C m^{-2} day (y = -0.77 x +6.7); overall decreasing the C sink strength (NEE) by an average of 0.53 g C m^{-2} day (y = 0.53 x -3.9). Therefore, horizon shade negatively impacted C uptake at the site.
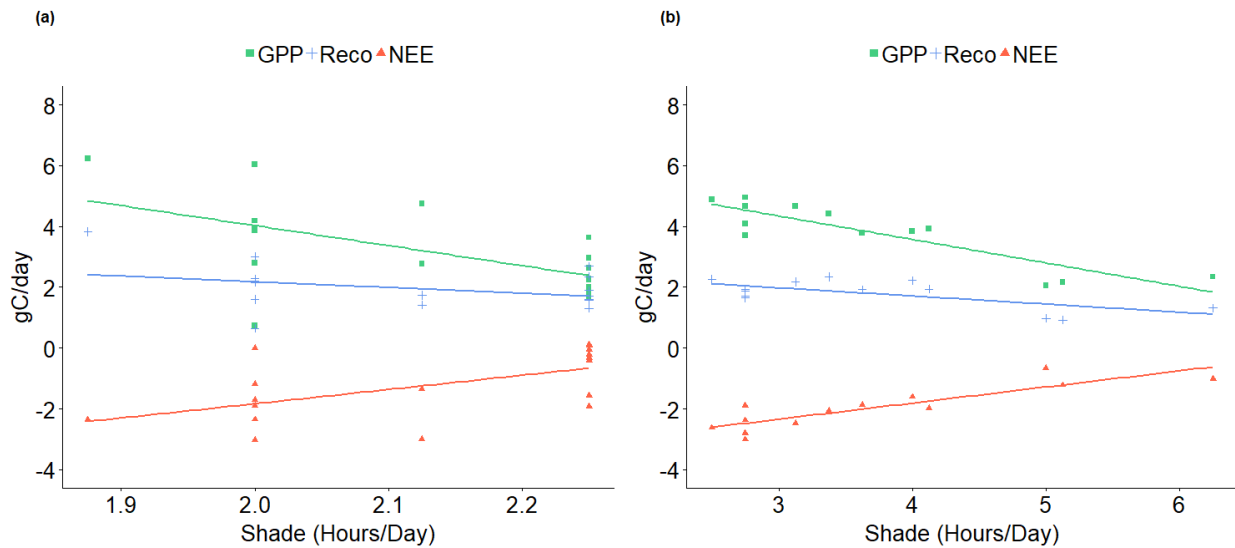
Figure 3-9: Relationship between hours of shade and components of the Carbon flux: Gross Primary Production (GPP), Ecosystem Respiration (R_{eco}), and Net Ecosystem Exchange (NEE) on Growing Season clear sky days during the periods of (a) *Stable Shade*, and (b) *Dynamic Shade* at Bonsai wetland, Fortress Mountain, Alberta, 2018.

The period of *Stable Shade* yielded non-significant and inconclusive results for ET, PET, and R_{eco} (Figure 3-7a; Figure 3-8a), indicating that there were other environmental variables influencing water and carbon fluxes in *Stable Shade,* when there was a similar amount of shade and K↓ per day. Therefore, VMC, T_a & T_s were added to the water and carbon analysis to determine their role on fluxes. ET was strongly influenced by VMC ($R^2 = 0.55$, $p < 0.001$), T_a ($R^2 = 0.53$, $p < 0.001$), and T_s ($R^2 = 0.66$, $p < 0.0001$). It was also found that T_a had a statistically significant positive relationship with GPP ($R^2 = 0.35$, $p < 0.001$), and a statistically significant negative relationship with NEE ($R^2 = 0.35$, $p < 0.01$) and R_{eco} ($R^2 = 0.23$, $p < 0.05$). T_s had a statistically significant positive relationship with GPP ($R^2 = 0.22$, $p < 0.05$), a statistically significant negative relationship with NEE ($R^2 = 0.46$, $p < 0.01$) and a non-significant relationship with R_{eco} ($R^2 = 0.007$, $p = 0.76$). Finally, soil moisture had a statistically significant negative relationship with GPP ($R^2 = 0.51$, $p < 0.01$), a statistically significant positive relationship with NEE ($R^2 = 0.55$, $p < 0.001$), and a non-significant relationship with R_{eco} ($R^2 = 0.02$, $p = 0.27$).

Figure 3-10 found similar results to the statistical analysis, in which ET and GPP were strongly influenced by the horizon shadow. In a uniform and non complex environment, fluxes display a normal bell curve pattern increasing in the morning, peaking in the afternoon, and decreasing into the evening. However, at Bonsai there was a noticeable shift from this pattern in

the middle of July, where half hourly ET had a sudden reduction at 16:00 hours. This trend became more intense into August, when shade decreased energy and water fluxes in the morning from 09:00 to 11:00 hours and at 15:00 hours in the afternoon. The response of ET to horizon shade followed a nearly identical pattern as K↓ and Q*, while GPP had a different seasonal and daily pattern. Similar to the results found in the statistical analysis, GPP did not follow the same pattern as ET, K↓, or Q* during constant shade, but did have a narrowing bell curve shape in the portion of increasing shade in *Peak Growing Season*. In general, carbon uptake through GPP was greatest midday from the middle of July to the middle of August between the hours of 08:00 and 18:00. In the middle of August there was a rapid decline in C uptake, as the wetland transitioned from 0.27 g C/30 mins to 0.06 - 0.13 g C/30 mins and closer to net neutral carbon uptake during daytime hours.
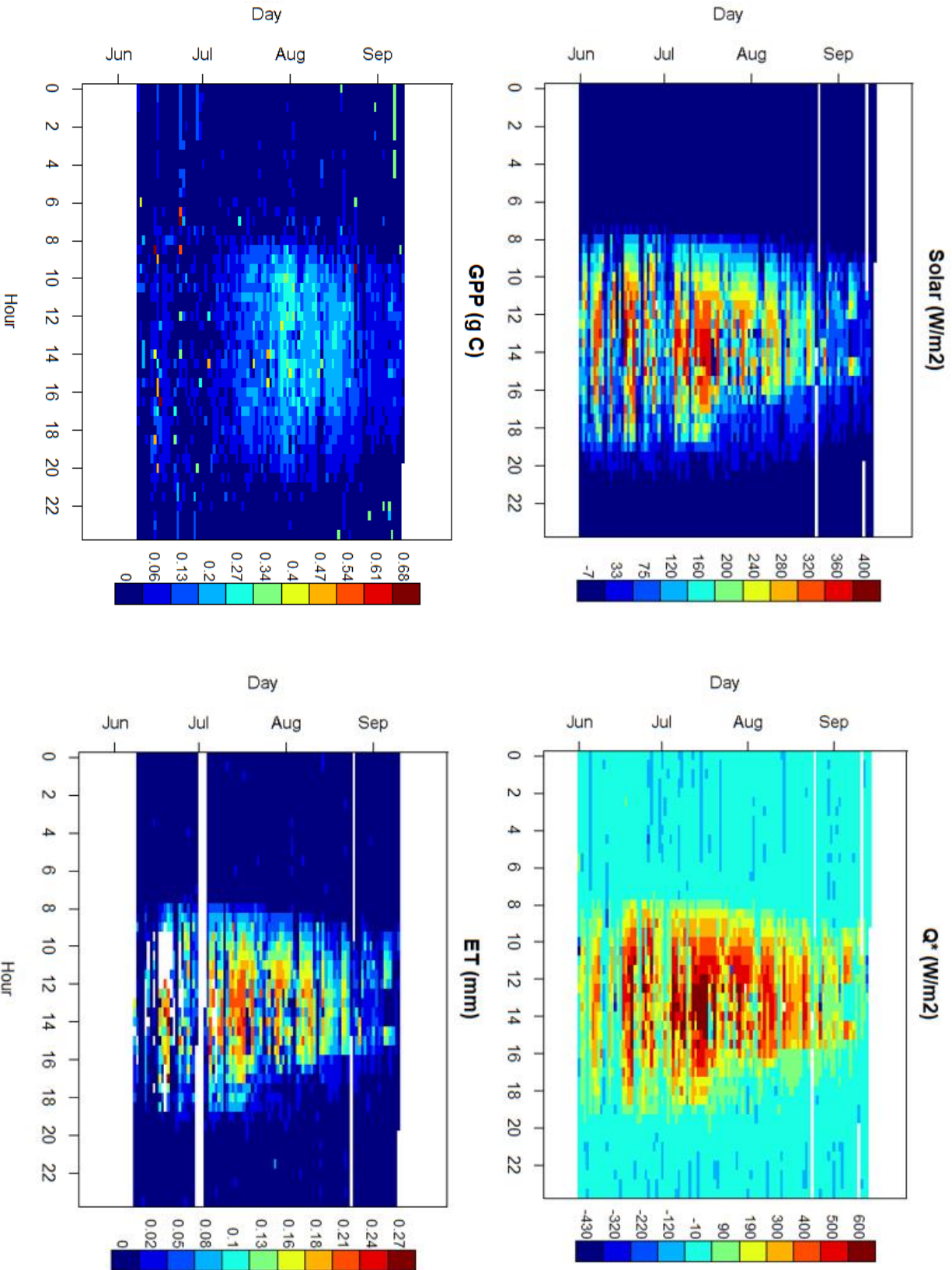
Figure 3-10: Seasonal energy, water, and carbon fluxes displayed in 30-minute timestamps. Energy flux is represented as solar radiation and net radiation (Q*) (W/m²), water flux is evapotranspiration (ET) (mm), and the carbon flux is Gross Primary Production (g C).

3.5 Discussion

3.5.1 Growing season evapotranspiration from a sub-alpine wetland

Bonsai had a significantly lower ET (157 mm) over the summer than other alpine meadows and wetlands (Flerchinger et al. 2010; Wu et al. 2015) because of its shorter growing season (Sanderson & Cooper, 2008; Wang et al. 2012). Recent literature suggests that subalpine wet meadows and wetlands have a large annual range in ET that may reach up to 994 mm, with growing season (May to October) contributions of 200 – 657 mm (Groeneveld et al. 2007; Sanderson & Cooper, 2008; Wu et al. 2015). Large seasonal differences in ET are often caused by localised environmental variables that alter season length, like solar radiation, air temperature, precipitation, water table depth, and soil moisture content (Flerchinger et al. 2010; Wu et al. 2015). In this study, low cumulative ET at Bonsai was due to the strong relationship between ET, available energy, and horizon shade. Throughout the measurement period shade supported a thick snowpack, delayed transpiration contributions to ET, and limited the available energy during critical daily and seasonal growth periods. The influence of shade is evident when Bonsai is compared to studies conducted at subalpine wetlands with similar vegetation structure, soil moisture, and water table depth. A wet meadow (3,885 m a.s.l.) in the Qinghai-Tibetan Plateau (QTP), China and a playas wetland (2,350 m a.s.l.) in San Luis Valley (SLV), Colorado each had higher seasonal ET with 236 mm (June to September) and 352 mm (April to October), respectively (Sanderson & Cooper, 2008; Wu et al. 2015). Both subalpine wetlands had cool average temperatures, low water tables, and vegetation dominated by sedges, grasses, and reeds; indicating that one of the limiting variables for low ET at Bonsai was horizon shade. The impact of horizon shade is visible when observing the hourly and daily patterns of water fluxes across the season.

Bonsai displayed similar seasonal ET patterns to the subalpine wetland, defined by increases through *Snow Melt*, peak ET flux during *Green Up,* and a steady decline in ET throughout *Peak Growing Season* into *Senescence* (Cooper et al. 2006; Sanderson & Cooper 2008; Wang et al. 2012). There was a spike in ET during the midday hours (12:00 to 17:00) of early June because of evaporation from snowmelt runoff (Figure 3-10). Following this, ET continued to increase until the seasonal maximum, which lasted from July 5th to 17th, two weeks before the literature (Cooper et al. 2006; Wu et al. 2015).   Seasonality differed between our study and the literature because the influence of shade grew as the season progressed. In the middle of July there

was a noticeable decrease in K↓ (200 to 75 W/m^2) and ET (0.13 to 0.05 mm) beginning at 16:00 hours (Figure 3-10). The decreasing hourly trend in K↓ and ET continued into August where shade began to influence fluxes in the afternoon (beyond 15:00 hours) and in the morning from 09:00 to 11:00 hours. During the afternoon, K↓ and ET should have declined until sunset; however, a sharp reduction at 16:00 hours in the middle of July indicated that the horizon shadow shaped the localized energy and water fluxes during the *Peak Growing Season* (Figure 3-10).

This study found that the seasonal water fluxes were strongly influenced by the relationship between available energy and the horizon shadow. The first manuscript of this thesis (Chapter 2) found that each hourly increase of shade during *Dynamic Shade*, reduced daily K↓ and Q* by 13% and 16 %, respectively. Since ET is largely controlled by the available energy, it was expected that shade would also strongly influence ET. During *Dynamic Shade*, each hourly interval of shade per day decreased ET by 17 %. Therefore, our study drew similar conclusions to the literature which found that lower ET aligned with periods of reduced available energy and higher shade (Oliphant, 2000). Since shade had a similar reduction on ET and Q* on clear sky days, it was an important control mechanism on the water and energy fluxes at Bonsai over the summer months.

3.5.2 Variability in sub-alpine wetland carbon flux

The C flux varied greatly over the study period as the system quickly shifted between a source and sink in response to changing environmental conditions following *Snow Melt*. When the surface was snow covered, the wetland behaved as a carbon source; however, as S*now Melt* progressed with greater temperature and soil moisture, vegetation productivity increased through *Green Up,* peaked during Peak *Growing Season,* and decreased into *Senescence*. Considering all seasonal phases, the study period was a cumulative net sink of 63 g C m^{-2} and was comparable to snow free period values reported in the alpine tundra, meadow, and wetland literature (Kato, et al. 2003; Zhao et al. 2010; Knowles et al. 2014; Millar et al. 2017). Average growing season NEE in alpine wetlands varied from strong sinks at the QTP (46 to 212 g C m^{-2}) (Kato et al. 2003; Kato et al. 2006; Zhao et al. 2010), to strong sources and sinks (-342 to 256 g C m^{-2}) in the Rocky Mountains of Wyoming and Colorado (Knowles et al. 2014; Millar et al. 2017). Although alpine systems have shown varying results in ecosystem source/sink strength, winter C flux studies have found the alpine meadow and wetland to be a strong C source when the ground surface is insulated by snow cover and heterotrophic soil respiration remains active (Zhao et al. 2010; Knowles et al.

2014; Lange et al. 2016). Results from this study found that insulation by the snowpack kept soil temperature (2 cm) above -5 °C during *Snow Melt,* meeting the threshold required for respiration to occur (Lange et al. 2016). This indicates that soil respiration likely continues over the winter months at Bonsai, making it an annual net source of C; however, an annual multi-year investigation would be required to quantify its average yearly net C contributions and confirm or refute this hypothesis.

Bonsai displayed normal seasonal trends in carbon flux with maximum GPP and R_{eco} during peak productivity. The measurement period began with a thick snowpack during *Snow Melt* that provided an insulating layer that resulted in "pulses" of carbon emission linked to precipitation, temperature, and degassing of air pores released during snowmelt. High heterotrophic soil respiration during the *Snow Melt* period resulted in a C source (averaging 1.4 g C m^{-2} day^{-1}) with the largest contributions occurring overnight in the middle of June from 22:00 to 06:00 hours. Because of a lengthy melt process, the *Green Up* period lasted longer than other alpine ecosystems and represented the increase in seasonal C flux that led to peak production during *Peak Growing Season*. The 2018 *Green Up* at Bonsai lasted from June 24th to July 20th, ending several weeks later than similar sites reported in literature: the QTP (Kato et al. 2004; Zhao et al. 2010) and Colorado Rocky Mountains (Knowles et al. 2014) wetlands began green up in June and ended by early July. This study had a shorter *Peak Growing Season* where the seasonal maximum in C uptake occurred two weeks later than literature, because *Green Up* entered the normal productive window found in alpine tundra, meadow, and wetland ecosystems (Kato et al. 2003; Zhao et al. 2010; Knowles et al. 2014). This indicates that the microclimate resulting from horizon shade extended *Green Up* and shortened *Peak Growing Season* by approximately two weeks.

Results from this study found that during the period of increasing shade, the C flux had a statistically significant relationship with the horizon shadow. During *Dynamic Shade*, GPP and R_{eco} had a statistically significant negative relationship with shade, while NEE had a statistically significant positive relationship with shade. Therefore, each hourly increase in shade per day during *Dynamic Shade*, decreased GPP by 15 % and increased NEE by 18 %, indicating that shade negatively impacted C uptake in this subalpine wetland. This finding was similar to other studies,

which found NEE to have a statistically significant relationship with K↓ ($p < 0.001$, $R^2 = 0.65$) (Kato et al. 2003; Cao et al. 2017).

In *Stable Shade*, when shade remained relatively constant, environmental variables like VMC, T_s, and T_a played a strong role in regulating the C flux (Kato et al. 2003; Zhao et al. 2010; Cao et al. 2017). Throughout *Stable Shade*, NEE increased with greater VMC from snowmelt and decreased with higher T_a and T_s during full leaf out, which is why the wetland was a net source in *Snow Melt* and early in *Green Up,* but a sink at the end of *Green Up* and throughout *Peak Growing Season.* Temperature and moisture have been identified in the literature to strongly influence NEE in alpine meadow and wetland ecosystems, in which temperature has been particularly recognized as an important photosynthetic cue (Monson et al. 2002; Knowles et al. 2014; Millar et al. 2017). The relationship between C and temperature was very noticeable as NEE increased alongside T_s through *Green Up* and *Peak Growing Season*, and quickly responded to an abnormal spike in T_a and T_s on September 7th in *Senescence.*

3.5.3 WUE as an indicator for sub-alpine wetland water use

Water use efficiency varied in response to changes in plant productivity and water availability. Over the course of the study, average WUE was comparable to alpine meadow and wetland literature (Hu et al. 2008; Zhu et al. 2014). Maximum WUE was an order of magnitude less and occurred several weeks later in the season than other studies (Hu et al. 2008; Monson et al. 2010; Zhu et al. 2014), while minimum WUE occurred during a similar timeframe found in the literature (Monson et al. 2010; Tian et al. 2010). The seasonal differences in WUE were attributed to a surplus of water resources during *Green Up* that supported high evaporative losses and low C production, while a lower water supply during *Peak Growing Season* was mainly used in photosynthesis. This indicates that although soil moisture decreased through the season, vegetation showed a greater WUE, suggesting that shaded valley wetlands remain productive through a short opportunity for growth. Recent studies have found that during the growing season, WUE increases linearly with lower K↓ and that fluctuations in light availability (i.e. horizon shade or cloud cover) increase plant productivity (Gao et al. 2018; Kromdijk et al. 2016). The findings from this study agree with the literature, that lower soil moisture and decreased K↓ led to a higher WUE over the entire study but found no direct relationship with shade during the period of *Dynamic Shade* (Niu

et al. 2011; Han et al. 2013; Gao et al. 2018). This confirms our hypothesis that WUE remained relatively unaffected because shade reduced ET and GPP by similar margins.

This study found the environmental variables that influence water and carbon fluxes equally control seasonal patterns of WUE. This is the result of a tightly interconnected ecosystem where shade and the resulting microclimate govern the ecohydrological conditions. Horizon shade sheltered a thick snow pack from rapid spring melt which slowly released water, maintained soil moisture, and supported evaporation early in the season. During *Peak Growing Season* shade reduced K↓ and decreased ET into *Senescence*. Therefore, horizon shade was a mechanism for moisture control because it supported an environment with increased snow accumulation and high VMC in the period of *Stable Shade* and low ET and GPP during *Dynamic Shade*. These patterns in water use indicate that the constrained growing season at Bonsai was supported by a horizon shadow that retained water to support the wetland during productive periods later in the season.

Under future climate uncertainties, water storage will become increasingly important in the subalpine zone, because forests have experienced increased disturbance, shortened growing seasons, decreased winter snow accumulation, and increased summer ET losses (Pomeroy et al. 2012; Harpold et al. 2015; Pomeroy et al. 2015). As a result, shaded wetlands provide an opportunity to store large volumes of water for late season runoff while remaining productive within short growing windows. Therefore, shade may delay or negate any rapid change(s) to wetland ecosystem functionality, which will help balance anticipated water losses from alpine forests. However, further research is required on SWE, to help understand snowmelt storage in wetlands and its contribution to downstream runoff.

3.6 Conclusions

This study analyzed the seasonal trends of water and C fluxes in a subalpine wetland and the role of horizon shade and other environmental variables on their temporal variability. Seasonal trends in ET and C found conflicting results with the literature. Cumulative ET was significantly lower, and the timing of seasonal maximum did not align with the literature. Peak C flux was also delayed compared to other studies because of a longer *Green Up* period that led to delayed peak production and a shorter *Peak Growing Season*. ET was highest in *Green Up*, while GPP was highest in *Peak Growing Season*, resulting from different controlling variables and water availability. ET and GPP

had strong relationships with shade that reduced the available energy for fluxes when shade increased as *Peak Growing Season* progressed. ET and C fluxes had a similar response to hourly increases in shade per day (ET 17 %, GPP 15 % reductions); however, ET responded faster to shade and was reduced by a larger margin, indicating that it had a lower energy cut-off threshold than GPP. Therefore, when shade was low and constant in *Stable Shade*, fluxes were largely influenced by environmental variables like T_a, T_s, and VMC; but, when shade increased rapidly in *Dynamic Shade*, it had a large influence on fluxes. With a seasonal average of 2.9 g C $(kg\ H_2O)^{-1}$, Bonsai had a low WUE that was comparable to the literature. Over the entire study period (June 7th to September 10th), WUE increased with decreasing soil moisture, but remained relatively unaffected by shade during the period of *Dynamic Shade* (July 30th to September 10th) because it equally reduced ET and GPP.

Overall, Bonsai water and C fluxes were largely reliant upon snowpack thickness, soil moisture, and available energy. The thick snowpack along the western margin of the wetland provided late season melt that maintained VMC and supported ET in *Green Up* and GPP during *Peak Growing Season.* However, sharp reductions in ET began in August when horizon shade grew in spatial extent and reduced available energy to the wetland. It is hypothesized that reduced evaporative losses helped support late season runoff to downstream communities where water supplies are needed (i.e. the prairies). However, we must further investigate SWE and isotope signatures to help quantify and identify late season runoff contributions from Bonsai to downstream systems.

Chapter 4:   Summary and Limitations

4.1 Summary

It is widely known that alpine regions will experience increased disturbance (i.e. wildfire, insect infestation, and disease) linked to changes in climate and human activity (Desai et al. 2011; Fang et al. 2013). Although the risk of drought and flooding increase in lowlands, there remains a lack of hydrological knowledge within alpine headwater catchments during the growing season. Historically, research at the headwater has focused on snow and glacial melt during transitional periods in spring and fall (Pluss & Mazzoni, 1994; Marks et al. 2008; Ma et al. 2016). Therefore, it is critical to develop a stronger understanding of water use and storage within the Canadian Rocky Mountains, because this region has already been subject to mountain pine beetle infestation and historic floods (i.e. Calgary 2013). To help establish effective planning and policy development, we must first increase our knowledge on the relationship between the energy and water fluxes of mountain ecosystems during the snow free period. Shade dynamics in alpine environments have been shown to significantly control radiation exchange (Oliphant et al. 2003; Marsh et al 2012); yet, this was the first in depth study to model seasonal shade patterns during the growing season and to determine how shade influences the energy, water and carbon fluxes of a subalpine wetland.

This research found that horizon shade varied in intensity and spatial extent over the growing season in relation to the sun path and surrounding topography. Early in the study, shade did not have a large influence over wetland hydroclimatology, averaging only 2 hours per day until July 30th. During *Stable Shade*, shade was more intense along the South-West boundary of the wetland, behaving as an important mechanism for moisture control. Shade reduced the radiative and turbulent fluxes, which supported a thicker snowpack that remained longer into the season than anywhere in the surrounding basin. However, when shade increased in the period of *Dynamic Shade*, components of the energy budget had a statistically significant negative relationship with the horizon shadow. On average, each hourly increase per day in horizon shade reduced Q^* and $K\downarrow$ by 28 W/m^2 and 32 W/m^2, equivalent to 16 % and 13 % of daily total energy, respectively. The water and carbon fluxes followed similar patterns as Q^* and $K\downarrow$, where each hour of shade reduced ET and GPP by 17 % and 15 %, respectively. ET had a faster response to shade, indicating that the threshold for energy required to sustain ET was lower than that of GPP. Water use

efficiency was not affected by the horizon shadow, because shade equally reduced ET and GPP. Low WUE in *Stable Shade* indicates that the wetland was highly saturated from snowmelt runoff, resulting in high evaporative contributions to ET but low carbon uptake from non-productive vegetation. However, once the snowpack dissipated, the wetland had a high WUE due to lower ET and higher GPP from vegetation in full leaf out.

This knowledge provides better insight in predicting the response of water and carbon use in subalpine wetlands to climate change. In general, subalpine wetlands have been vastly under-represented in water and carbon flux literature, making the observed measurements from this study an important contribution to help establish a working knowledge of baseline conditions within these systems. Therefore, the insights and conclusions drawn from this research will help gap fill regional water budgets through enhanced models with an increased understanding of ecohydrological conditions in subalpine wetlands. Finally, increased knowledge on shade within mountain catchments will enhance modelling techniques by improving our understanding of energy, water, and carbon fluxes within ecosystems surrounded by complex terrain.

4.2 Project Limitations

This study encountered some limitations that are important to address. The hill shade model in ArcMap (v10.6) provided a useful tool to help quantitatively analyze the spatial and temporal patterns in shade across the study site. However, the model assumed clear sky conditions with no indication of fog, smoke, or overcast skies. Therefore, observed data was filtered for days that met these requirements by analyzing daily field notes and trends in solar radiation. Only days that had clear skies in the field notes and near perfect bell curves in observed solar radiation were included in the study. This reduced the sample size by approximately 32% from 96 sample days to 31 sample days, which remained an adequate sample size to conduct statistical analysis (Minitab, 2017).

Appendix 1: Eddy Covariance Processing Method

Raw EC data was processed internally by the datalogger using the Easy Flux software provided by Campbell Scientific within their data loggers, which accounted for Webb density (Webb et al. 1980) correction for open path sensors. Due to limited storage, only final fluxes were stored on the data logger and not high frequency data. Once fluxes and meteorological data were downloaded and compiled for the study period, they were processed in R-Software using a custom-made script, where data was quality checked and flagged for record completeness and outliers, following suggested methods in Aubinet et al (2012). Additionally, half-hourly averages that measured rain and corresponded to environmental conditions favourable for dew formation (calculated from meteorological data) were flagged as missing values in analysis. A footprint analysis was then completed for the study site following Kljun et al 2015 (using their FFP R-functions). All fluxes were then filtered to be from within 80% of the calculated footprint (Figure A-1). The data located within the footprint was then processed further, where C-fluxes were partitioned and gapfilled and water fluxes were gapfilled. Carbon flux data was partitioned into component fluxes of gross primary production (GPP) and ecosystem respiration (R_{eco}), while Net Ecosystem Exchange (NEE) was subsequently gapfilled, using the REddyProc R-package of Wurtzler et al (2018). Sensible and latent heat fluxes within the footprint of the tower were processed following standard protocols found in Petrone et al. (2001), Wilson et al. (2002), Brown et al. (2010), and Petrone et al. (2015). ET was calculated from latent heat flux and gapfilled using the Bowen ratio method and Prisetly Taylor calculated ET, following Petrone et al. (2001). Ground heat flux was gapfilled as 10% of measured net radiation.
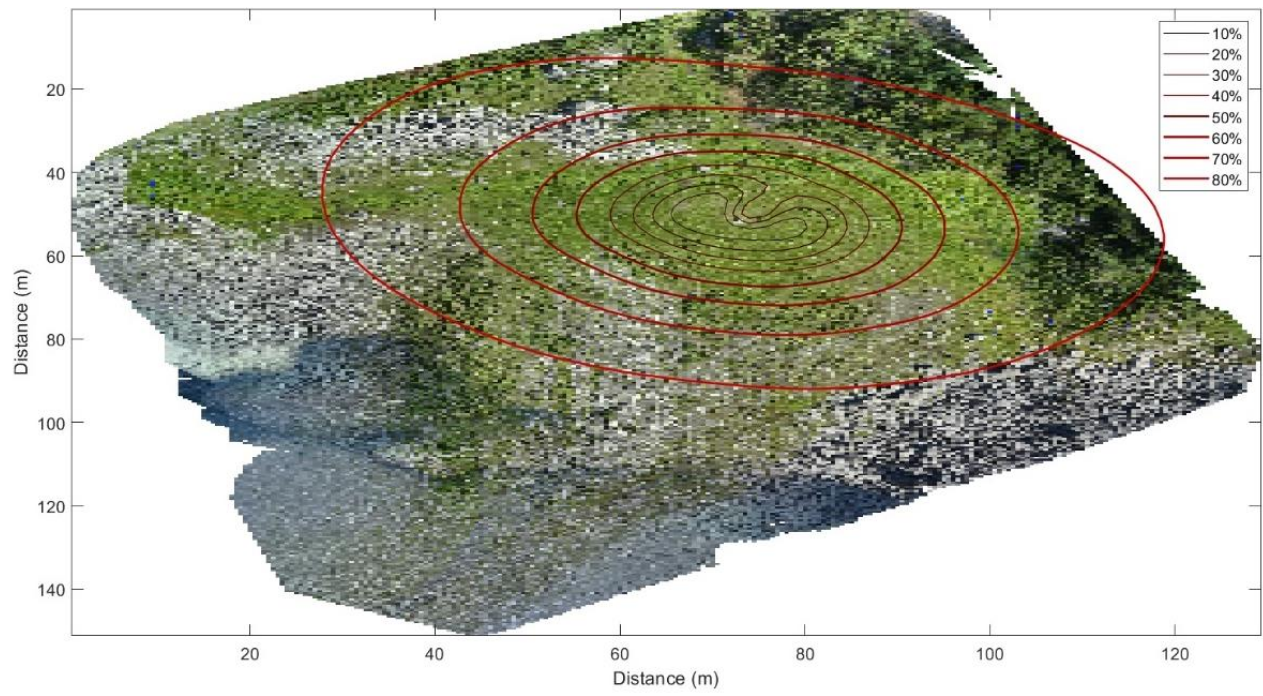
Figure A-1: Average Eddy Covariance flux footprint map over the study period.

References

Aber, J., Pavri, F., & Aber, S. (2012). High-latitude and high-altitude wetland case studies. *Wetland Environments: A Global Perspective*, 336–357.

Ackerly, D. D. (2010). The geography of climate change: implications for conservation biogeography. *Diversity and Distributions, 16*(3), 476-487.

Alberta Environment and Parks, Government of Alberta. (2018). Base Watersheds. Edmonton, Alberta: Alberta Environment and Parks, Government of Alberta. Retrieved from https://www.alberta.ca/hydrological-data.aspx

Ashfaq, M., Ghosh, S., Kao, S. C., Bowling, L. C., Mote, P., Touma, D., . . . Diffenbaugh, N. S. (2013). Near term acceleration of hydroclimatic change in the western US. *Journal of Geophysical Research: Atmospheres, 118*(10), 676–693.

Aubinet, M., Vesala, T., & Papale, D. (2012). *Eddy covariance: a practical guide to measurement and data analysis.* Springer & Business Media.

Badano, E. I., Cavieres, L. A., Molina-Montenegro, M. A., & Quiroz, C. L. (2005). Slope aspect influences plant association patterns in the Mediterranean matorral of central Chile. *Journal of Arid Environments, 62*(1), 93-108.

Bales, R. C., Molotch, N. P., Painter, T. H., Dettinger, M. D., Rice, R., & Dozier, J. (2006). Mountain hydrology of the western United States. *Water Resources Research, 42*, 1-13.

Barnett, T. P., Adam, J. C., & Lettenmaier, D. P. (2005). Potential impactsof a warming climate on water availability in snow-dominated region. *Nature, 438*, 303-309.

Baron, J. S., Schmidt, T. M., & Hartman, M. D. (2009). Climate-induced changes in high elevation stream nitrate dynamics. *Global Change Biology, 15*, 1777–1789.

Barros, C., Gueguen, M., Douzet, R., Carboni, M., Boulangeat, I., Zimmermann, E. N., & Thuiller, W. (2017). Extreme climate events counteract the effects of climate and land-use changes in alpine treelines. *Journal of Applied Ecology, 54*(1), 39-50.

Barry, R. G. (1981). *Mountain Weather and Climate.* London: Methuen & Co.

Bavay, M., Grunewald, T., & Lehning, M. (2015). Response of snow cover and runoff to climate change in high alpine catchments of Eastern Switzerland. *Advances in Water Resources, 55*, 4-16.

Beniston, M. (2003). Climatic change in mountain regions: a review of possible impacts. *Climatic Change, 59*, 5-31.

Beniston, M. (2006). Mountain weather and climate: A general overview and a focus on climatic change in the Alps. *Hydrobiologia, 562*, 3-16.

Benniea, J., Huntleya, B., Wiltshirea, A., Hillb, M. O., & Baxter, R. (2008). Slope, aspect and climate: Spatially explicit and implicit models of topographic microclimate in chalk grassland. *Ecological Modelling, 216*(1), 47-59.

Böhm, R., Auer, I., Brunetti, M., Maugeri, M., Nanni, T., & Schöner, W. (2001). Regional temperature variability in the European Alps: 1760–1998 from homogenized instrumental time series. *International Journal of Climatology, 21*, 1779–1801.

Brown, R. D., & Robinson, D. A. (2011). Northern Hemisphere spring snow cover variability and change over 1922–2010 including an assessment of uncertainty. *The Cryosphere, 5*, 219-229.

Brown, S. M., Petrone, R. M., Mendoza, C., & Devito, K. J. (2010). Surface vegetation controls on evapotranspiration from a sub humid Western Boreal Plain wetland. *Hydrological Processes, 24*(8), 1072-1085.

Bush, E., & Lemmen, D. (Eds.). (2019). Canada's Changing Climate Report. *Government of Canada*, 444.

Calgary Foundation. (2019). *Land Acknowledgement*. Retrieved from Calgary Foundation: For Community, Forever: https://calgaryfoundation.org/about-us/vital-priorities/strengthening-relationships-with-indigenous-communities/land-acknowledgement/?fbclid=IwAR3S0eLUkNtMVpenUUycoJLriPmcfaE0viCpK_uH51FBxLvuhpZeSjnftZk

Campbell, D. I., & Williamson, J. L. (1997). Evaporation from a raised peat bog. *Journal of Hydrology, 193*, 142–160.

Cannone, N., Sgorbati, S., & Guglielmin, M. (2007). Unexpected impacts of climate change on alpine vegetation. *Frontiers in Ecology and the Environment, 5*(7), 360–364.

Cao, S., Cao, G., Feng, Q., Han, G., Lin, Y., Yuan, J., . . . Cheng, S. (2017). Alpine wetland ecosystem carbon sink and its controls at the Qinghai Lake. *Environmental Each Sciences, 76*(210), 1-15.

Chen, L.-F., He, Z.-B., Du, J., Hang, J.-J., & Zhu, X. (2016). Patterns and environmental controls of soil organic carbon and total. *Catena, 137*, 37-43.

Christensen, C. W. (2017, July). *A geophysical study of alpine groundwater processes and their geologic controls in the southeastern Canadian Rocky Mountains (Masters Thesis).*

Christensen, N. S., & Lettenmaier, D. P. (2007). A multitude ensemble approach to assessment of climate change impacts on the hydrology and water resources of the Colorado River Basin. *Hydrol. Earth Syst. Sci., 11*, 1417-1434.

Cooper, D. J., Sanderson, J. S., Stannard, D. I., & Groeneveld, D. P. (2006). Effects of long-term water table drawdown on evapotranspiration and vegetation in an arid region phreatophyte community. *Journal of Hydrology, 325*(1-4), 21-34.

Dean, W. E. (1974). Determination of carbonate and organic matter in calcareous sediments and sedimentary rocks by loss on ignition; comparison with other methods. *Journal of Sedimentary Research, 44*(1), 242-248.

DeBeer, C. M., & Pomeroy, J. W. (2009). Modelling snow melt and snowcover depletion in a small alpine cirque, Canadian Rocky Mountains. *Hydrological Processes, 23*(18), 2584–2599.

Desai, A. R., Moore, D. J., Ahue, W. K., Wilkes, P. T., de Wekker, S. F., Brooks, B. G., . . . al., e. (2011). Seasonal pattern of regional carbon balance in the central Rocky Mountains from surface and airborne measurements. *Journal of Geophysical Research, 116*.

Dymond, C. (2002). Mapping vegetation spatial patterns from modeled water, temperature and solar radiation gradients. *Journal of Photogametry and Remote Sensing, 57*(1-2), 69–85.

Ebrahimi, S., & Marshall, S. J. (2016). Surface energy balance sensitivity to meteorological variability on Haig Glacier, Canadian Rocky Mountains. *The Cryosphere, 10*, 2799–2819.

Essery, R., & Marks, D. (2007). Scaling and parametrization of clear-sky solar radiation over complex topography. *Journal of Geophysical Research, 112*, 1–12.

European Environment Agency. (2010, September 9). Europe's ecological backbone: recognising the true value of our mountains. *European Environment Agency*, 13-244.

Falge, E., Baldocchi, D., Olson, R., & Anthoni, P. (2001). Gap filling strategies for defensible annual sums of net ecosystem exchange. *Agric. For. Meteorol., 107*, 43-69.

Fang, X., Pomeroy, J. W., Ellis, C. R., MacDonald, M. K., DeBeer, C. M., & Brown, T. (2013). Multi-variable evaluation of hydrological model predictions for a headwater basin in the Canadian Rocky Mountains. *Hydrology and Earth System Sciences, 17*(4), 1635-1639.

Flerchinger, G. N., Marks, D., Reba, M. L., Yu, Q., & Seyfried, M. S. (2010). Surface fluxes and water balance of spatially varying vegetation within a small mountainous headwater catchment. *Hydrology and Earth System Sciences, 14*(6), 965-978.

Freeze, R. A., & Cherry, J. A. (1979). *Groundwater.* Englewood Cliffs, N.J.: Prentice-Hall Inc.

Gao, X., Gu, F., Mei, X., Hao, W., Li, H., & Gong, D. (2018). Light and water use efficiency as influenced by clouds and/or aerosols in a rainfed spring maize cropland on the loess plateau. *Crop Science, 58*(2), 853-862.

Geiger, R. (1965). *The Climate Near the Ground.* Cambridge, Massachusetts: Harvard University Press.

Gottfried, M., Pauli, H., & Grabherr, G. (1998). Prediction of vegetation patterns at the limits of plant life: a new view of the alpine–nival ecotone. *Arctic and Alpine Research, 30*, 207–221.

Graae, B. J., De Frenne, P., Kolb, A., Brunet, J., Chabrerie, O., Verheyen, K., . . . Milbau, A. (2012). On the use of weather data in ecological studies along altitudinal and latitudinal gradients. *Oikos, 121*(1), 3-19.

Grabherr, G., Gottfried, M., & Pauli, H. (1994). Climate effects on mountain plants. *Nature, 369*, 448.

Groeneveld, D. P., Baugh, W. M., Sanderson, J. S., & Cooper, D. J. (2007). Annual groundwater evapotranspiration mapped from single satellite scenes. *Journal of Hydrology, 344*(1-2), 146-156.

Grusson, Y., Sun, X., Gascoin, S., Sauvage, S., Raghavan, S., Anctil, F., & Sáchez-Pérez, J.-M. (2015). Assessing the capability of the SWAT model to simulate snow, snow melt and streamflow dynamics over an alpine watershed. *Journal of Hydrology, 531*, 574-588.

Gu, L., Baldocchi, D., Vernma, S. B., Black, T. A., Vesala, T., Falge, E. M., & Dowty, P. R. (2002). Advantages of diffuse radiation for terrestrial ecosystem productivity. *Journal of Geophysical Research, 107*(D6), ACL 2-1-ACL 2-23.

Han, Q., Luo, G., Li, C., Ye, H., & Chen, Y. (2013). Modeling grassland net primary productivity and water-use efficiency along an elevational gradient of the Northern Tianshan Mountains. *Journal of Arid Land, 5*(3), 354-365.

Harpold, A. A., Molotch, N. P., Musselman, K. N., Bales, R. C., Kirchner, P. B., Litvak, M., & Brooks, P. D. (2014). Soil moisture response to snowmelt timing in mixed-conifer subalpine forests. *Hydrological Processes, 29*(12), 2782-2798.

Hoffmann, T. (2018, May 1). Retrieved from SunCalc: https://www.suncalc.org/

Hu, Z., Yu, G., Fu, Y., Sun, X., Li, Y., Shi, P., . . . Zheng, Z. (2008). Effects of vegetation control on ecosystem water use efficiency within and among four grassland ecosystems in China. *Global Change Biology, 14*, 1609-1619.

Immerzeel, W. (2008). Spatial modeling of mountainous basins: An integrated analysis of the hydrological cycle, climate change and agriculture. *Netherlands Geographical Studies, 369*.

IPCC (Intergovernmental Panel on Climate Change). (2001). Third assessment report of the Intergovernmental Panel on Climate Change.

Ives, J. D., & and Messerli, B. (1999). Declared by United Nations as ''International Year of the Mountains". *Arctic, Antarctica, and Alpine Research, 3*, 211-213.

Kato, T., Tang, Y., Gu, S., Cui, X., Hirota, M., Du, M., . . . Oikawa, T. (2003). Carbon dioxide exchange between the atmosphere and an alpine meadow ecosystem on the Qinghai-Tibetan Plateau, China. *Agricultural and Forest Meteorology, 124*(1-2), 121-134.

Kato, T., Tang, Y., Gu, S., Hirota, M., Dus, M., Li, Y., & Zhao, X. (2006). Temperature and biomass influences on interannual changes in CO2 exchange in an alpine meadow on the Qinghai-Tibetan Plateau. *Global Change Biology, 12*(7), 1285-1298.

Kljun, N., Calanca, P., Rotach, M. W., & Schmid, H. P. (2015). A simple two-dimensional parameterisation for Flux Footprint Prediction (FFP). *Geoscience Model Development, 8*, 3695-3713.

Knowles, J. F., Burns, S. P., Blanken, P. D., & Monson, R. K. (2015). Fluxes of energy, water, and carbon dioxide from mountain ecosystems at Niwot Ridge, Colorado. *Plant Ecology & Diversity, 8*(5-6), 663–676.

Konzelmann, T., Calanca, P., Muller, G., Menzel, L., & Lang, H. (1997). Energy Balance and Evapotranspiration in a High Mountain Area during Summer. *Journal of Applied Meteorology, 36*, 966-973.

Kromdijk, J., Glowacka, K., Leonelli, L., Gabilly, S. T., TIawai, M., Niyogi, K. K., & Long, S. P. (2016). Improving photosynthesis and crop productivity by accelerating recovery from photoprotection. *Science, 354*(6314), 857-861.

Kullman, L. (2002). Rapid recent range-margin rise of tree and shrub species in the Swedish Scandes. *Journal of Ecology, 90*, 68-77.

Lange, S. F., Allaire, S. E., Castillo, M. A., & Dutillel, P. (2016). N2O and CO2 dynamics in a pasture soil across the frozen period. *Canadian Journal of Soil Science, 97*(3), 497-511.

Lapp, S., Byrne, J., Townshend, I., & Kienzle, S. (2005). Climate warming impacts on snow accumulation in an alpine watershed. *International Journal of Climatology, 25*(4), 521-536.

Larcher, W. (2006). *Physiological Plant Ecology* (4th ed.). Berlin: Springer.

LeDrew, E. F. (1975). The energy balance of a mid-latitude alpine site during the growing season. *Arctic and Alpine Research, 7*, 301-314.

Lenoir, J. (2013). Local temperatures inferred from plant communities suggest strong spatial buffering of climate warming across Northern Europe. *Global Change Biology, 19*(5), 1470-1481.

Ma, Y., Pinker, R. T., Wonsick, M. M., & Li, C. (2016). Shortwave Radiative Fluxes on Slopes. *Journal of Applied Meteorology and Climatology, 55*, 1513-1532.

Marks, D., Winstral, A., & Flerchinger, G. (2008). Comparing Simulated and Measured Sensible and Latent Heat Fluxes over Snow under a Pine Canopy to Improve an Energy Balance Snowmelt Model. *Journal of Hydrometeorology, 9*, 1506-1522.

Marsh, C. B., Pomeroy, J. W., & Spiteri, R. J. (2012). Implications of mountain shading on calculating energy for snowmelt using unstructured triangular meshes. *Hydrological Processes, 26*, 1767–1778.

McFarlane, J. C., & Sager, J. C. (1998). *Plant Growth Chamber Handbook.* (R. W. Langhans, & T. W. Tibbitts, Eds.) Ames, Iowa, USA: North Central Region Research Publication No.340: Chapter 1 - Radiation.

Medrano, H., Tomas, M., Martorell, S., Flexas, J., Hernandez, E., Rossello, A. P., . . . Bota, J. (2015). From leaf to whole-plant water use efficiency (WUE) in complex canopies: Limitations of leaf WUE as a selection target. *The Crop Journal, 3*(3), 220-228.

Meybeck, M., Green, P., & Vorosmarty, C. (2001). A new typology for mountains and other relief classes: an application to global continental water resources and population distribution. *Mountain Research and Development, 21*, 34–45.

Millar, D. J., Cooper, D. J., Dwire, K. A., Hubbard, R. M., & von Fischer, J. (2017). Mountain Peatlands Range from CO2 Sinks at High Elevations to Sources at Low Elevations: Implications for a Change Climate. *Ecosystems, 20*, 416–432.

Minitab. (2017). 1-Sample t-Test. *Minitab Assistant White Paper*, 1-18. Retrieved from https://support.minitab.com/en-us/minitab/18/Assistant_One_Sample_t.pdf

Monson, R. K., Turnipseed, A. A., Sparks, J. P., Harley, P. C., Scott-Denton, L. E., Sparks, K., & Huxman, T. E. (2002). Carbon sequestration in a high-elevation, subalpine forest. *Global Change Biology, 8*(5), 459-478.

Moore, D. J., Hu, J., Sacks, W. J., Schimel, D. S., & Monson, R. K. (2008). Estimating transpiration and the sensitivity of carbon uptake to water availability in a subalpine forest using a simple ecosystem process model informed by measured net CO2 and H2O fluxes. *Agricultural and Forest Meteorology, 148*(10), 1467-1477.

Niu, S., Xing, X., Zhang, Z., Xia, J., Xhou, X., Song, B., . . . Wan, S. (2011). Water-use efficiency in response to climate change: from leaf to ecosystem in a temperate steppe. *Global Change Biology, 17*(2), 1073-1082.

Oke, T. (1987). *Boundary Layer Climates* (Second ed.). New York: Methuen & Co Limited.

Oliphant, A. J. (2000). Spatial and temporal variability of surface energy fluxes in an alpine catchment. *Ph.D. Dissertation*, 199 pp.

Oliphant, A. J., Spronken-Smith, R. A., Sturman, A. P., & Owens, I. F. (2003). Spatial Variability of Surface Radiation Fluxes in Mountainous Terrain. *American Meteorological Society, 42*(1), 113-128.

Onipchenko, V., Blinnikov, M. S., & Aksenova, A. A. (2001). Experimental Evaluation of Shading Effects in Seasonal Dynamics of Four Alpine Communities in Northwestern Caucasus, Russia. *Arctic, Antarctic, and Alpine Research, 33*(3), 330-339.

Papale, D., Reichstein, M., Canfora, E., Aubinet, M., Bernhofer, C., Longdoz, B., . . . Yakir, D. (2006). Towards a more harmonized processing of eddy covariance CO2 fluxes: algorithms and uncertainty estimation. *Biogeosciences Discussion, 3*, 961-992.

Parker, B. R., Vinebrooke, R. D., & Schindler, D. W. (2008). Recent climate extremes alter alpine lake ecosystems. *Proceedings of the National of Sciences of the United States of America, 105*(35), 12927–12931.

Pauli, H., Gottfried, M., & Grabherr, G. (1999). Vascular plant distribution patterns at the low temperature limits of plant life – the alpine–nival ecotone of Mount Schrankogel (Tyrol, Austria). *Phytocoenologia, 29*, 297–325.

Petrone, R. M., Waddington, J. M., & Price, J. S. (2001). Ecosystem scale evapotranspiration and net CO2 exchange from a restored peatland. *Hydrological Processes, 15*(14), 2839-2845.

Petrone, R., Chasmer, L., Hopkinson, C., Silins, U., Landhausser, S., Kljun, N., & Devito, K. (2015). Effects of harvesting and drought on CO2 and H2O fluxes in an aspen-dominated western boreal plain forest:early chronosequence recovery. *Canadian Journal of Forest Research, 45*(1), 87-100.

Pluss, C., & Mazzoni, R. (1994). The role of turbulent heat fluxes in the energy balance of high alpine snow cover. *Nordic Hydrology, 25*, 25-38.

Pomeroy, J. W., Fang, X., & Ellis, C. (2012). Sensitivity of snowmelt hydrology in hydrology in Marmot Creek, Alberta to forest cover disturbance. *Hydrological Processes, 26*(12), 1892-1905.

Pomeroy, J. W., Fang, X., & Rasouli, K. (2015). Sensitivity of snow processes to warming in the Canadian Rockies. *72nd Eastern Snow Conference*, (pp. 22-33). Sherbrooke, Quebec, Canada.

Pomeroy, J., Toth, B., Granger, R., Hedstrom, N., & Essery, R. (2003). Variation in surface energetics during snowmelt in a subarctic mountain catchment. *Journal of Hydrometeorology, 4*(4), 702–719.

Priestley, C. H., & Taylor, R. J. (1972). On the Assessment of Surface Heat Flux and Evaporation Using Large-Scale Parameters. *Monthly Weather Review, 100*(2), 81-92.

Quan, Q., Zhang, F., Tian, D., Zhou, Q., Wang, L., & Niu, S. (2018). Transpiration Dominates Ecosystem Water-Use Efficiency in Response to Warming in an Alpine Meadow. *Journal of Geophysical Research: Biogeosciences, 123*, 453-462.

Regonda, S. K., Rajagopalan, B., Clark, M., & Pitlick, J. (2004). Seasonal cycle shifts in hydroclimatology over the western United States. *Journal of Climatology, 18*, 372–384.

Rocha, A. V., & Goulden, M. L. (2009). Why is marsh productivity so high? New insights from eddy covariance and biomass measurements in a Typha marsh. *Agricultural and Forest Meteorology, 149*(1), 159-168.

Rood, S. B., Pan, J., Gill, K. M., Franks, C. G., Samuelson, G. M., & Shepherd, A. (2008). Declining summer flows of Rocky Mountain rivers: Changing seasonal hydrology and probable impacts on foodplain forests. *Journal of Hydrology, 349*, 397–410.

Rooney, R., Bolding, M., & Lei, C. (2018 unpublished). Vegetation Survey at Bonsai 2018. *Unpublished Data*.

Rosenberg, N. J., Blad, B. L., & Verma, S. B. (1983). *Microclimate, the biological environment* (2 ed.). New York: John Wiley & Sons.

RStudio Team. (2016). RStudio: Integrated Development Environment for R. Bonston, MA: RStudio, Inc. Retrieved from http://www.rstudio.com/

Sanderson, J. S., & Cooper, D. J. (2008). Ground water discharge by evapotranspiration in wetlands of an arid intermountain basin. *Journal of Hydrology, 351*(3-4), 344-359.

Scherrer, D., & Korner, C. (2011). Topographically controlled thermal-habitat differentiation buffers alpine plant diversity against climate warming. *Journal of Biogeography, 38*(2), 406-416.

Schimel, D., Kittel, T. G., Running, S., Monson, R., Turnipseed, A., & Anderson, D. (2002). Carbon sequestration studied in western U.S. mountains. *EOS: American Geophysical Union, 83*(40), 445-449.

Souch, C., Wolfe, C. P., & Grimmond, C. S. (1996). Wetland evaporation and energy partitioning: Indiana Dunes National Lakeshore. *Journal of Hydrology, 184*, 189–208.

Spokas, K., & Forcella, F. (2006). Estimating hourly incoming solar radiation from limited meteorological data. *Weed Science, 54*(1), 182-189.

St. Jacques, J.-M., Sauchyn, D. J., & Zhao, Y. (2010). Northern Rocky Mountain streamflow records: Global warming treands, human impacts or natural variability? *Geophysical Research Letters, 37*(6).

Statistics Canada. (2018, March 12). *Statistics Canada*. Retrieved from 2016 Census - Boundary files: https://www12.statcan.gc.ca/census-recensement/2011/geo/bound-limit/bound-limit-2016-eng.cfm?fbclid=IwAR0h5jZvoWNjHIAby4tbaoiFrMZKXpZ3_mf32AJbIky-AqcvXOY4tnqcTJ8

Stewart, I. T., Cayan, D. R., & Dettinger, M. D. (2004). Changes in snowmelt runoff timing in western North America under a "business as usual" climate change scenario. *Climatic Change, 62*(1-3), 217-232.

Storr, D. (1967). Precipitation variations in a small forested watershed. *Proc 35th AnnualWestern Snow Conference*, (pp. 11–17). Boise, Idaho.

Strobl, S., Cueva, E., Silva, B., Knuesting, J., Schorsch, M., Schneibe, R., . . . Beck, E. (2017). Water relations and photosynthetic water use efficiency as indicators of slow climate change effects on trees in a tropical mountain forest in South Ecuador. *Ecological Indicators, 83*, 550-558.

Sulman, B., Desai, A., Cook, B., Saliendra, N., & Mackay, D. (2009). Contrasting carbon dioxide fluxes between a drying shrub wetland in Northern Wisconsin, USA, and nearby forests. *Biogeosciences, 6*(6), 1115-1126.

Theurillat, J. P., & Guisan, A. (2001). Potential impact of climate change on vegetation in the European Alps: a review. *Climatic Change, 50*(1-2), 77–109.

Thimijan, R. W., & Heins, R. D. (1983). Photometric, radiometric and quantum light units of measure: A review of procedures for interconversion. *Horticultural Science, 18*(6), 818-822.

Tian, H., Chen, G., Liu, M., Zhang, C., Sun, G., Lu, C., . . . Chappelka, Z. (2010). Model estimates of net primary productivity, evapotranspiration, and water use efficiency in the terrestrial ecosystems of the Southern United States during 1895-2007. *Forest Ecology and Management, 259*, 1311-1327.

Turnipseed, A. A., Blanken, P. D., Anderson, D. E., & Monson, R. K. (2002). Energy budget above a high-elevation subalpine forest in complex topography. *Agricultural and Forest Meteorology, 110*, 177–201.

Urban, O., Janous, D., Acosta, M., Czerny, R., Markova, I., Navratil, M., . . . Marek, M. V. (2007). Ecophysiological controls over the net ecosystem exchange of mountain spruce stand. Comparison of the response in direct vs. diffuse solar radiation. *Global Change Biology, 13*(1), 157-168.

Viviroli, D., Archer, D., Buytaert, W., Fowler, H., Greenwood, G., Hamlet, A., . . . Woods, R. (2011). Climate change and mountain water resources: overview and recommendations for research, management and policy. *Hydrology and Earth System Science, 15*, 471-504.

Walther, G. R., Beißner, S., & Burga, C. A. (2005). Trends in the upward shift of alpine plants. *Journal of Vegetation Science, 16*, 541–548.

Wang, Y. L., Wang, X., Zheng, Q. Y., & Guo, X. J. (2012). A Comparative Study on Hourly Real Evapotranspiration and Potential Evapotranspiration during Different Vegetation Growth Stages in the Zoige Wetland. *Procedia Environmental Sciences, 13*, 1585-1594.

Webb, E. K., Pearman, G. I., & Leuning, R. (1980). Correction of flux measurements for density effects due to heat and water vapour transfer. *Royal Meteorological Society, 106*(447), 85-100.

Wickland, K. P., Striegl, R. G., Mast, M. A., & Clow, D. W. (2001). Carbon gase xchangea t a southernR ockyM ountain wetland, 1996-1998. *Global Biogeochemical Cycles, 15*(2), 321-335.

Wilson, K., Goldstein, A., Falge, E., Aubinet, M., Baldocchi, D., Berbigier, P., . . . Verma, S. (2002). Energy balance closure at FLUXNET sites. *Agricultural Forest Meteorology, 113*, 223-243.

Windell, J. T., Willard, B. E., Cooper, D. J., Foster, S. Q., Knud-Hansen, C. F., Rink, L. P., & Kiladis, G. N. (1986). Wetlands, An Ecological Characterization of Rocky Mountain Montane and Subalpine. *U. S. Fish & Wildlife Service Biological Report, 86*(11), 298 pp.

Wu, J.-k., Zhang, S.-q., Wu, H., Liu, S.-w., Qin, Y., & Qin, J. (2015). Actual Evapotranspiration in Suli Alpine Meadow in Northeastern Edge of Qinghai-Tibet Plateau, China. *Advances in Meteorology*, 1-10.

Wurtzler, T., Lucas-Moffat, A., Migliavacca, M., Knauer, J., Sickel, K., Sigut, L., . . . Reichstein, M. (2018). Basic and extensible post-processing of eddy covariance flux data with REddyProc. *Biogeosciences, 15*(16), 5015-5030.

Zhao, L., Li, J., Xu, S., Zhou, H., Li, Y., Gu, S., & Zhao, Z. (2010). Seasonal variations in carbon dioxide exchange in an alpine wetland meadow on the Qinghai-Tibetan Plateau. *Biogeosciences, 7*, 1207-1221.

Zhu, X., Yu, G., Wang, Q., Hu, Z., Han, S., Yan, J., . . . Zhao, L. (2014). Seasonal dynamics of water use efficiency of typical forest and grassland ecosystems in China. *Journal of Forest Research, 19*(1), 70-76.